ACIBADEM MEHMET ALI AYDINLAR UNIVERSITY
INSTITUTE OF HEALTH SCIENCES

UNRAVELING NEW BINDING PARTNERS OF ATG3 IN AUTOPHAGY AND MITOPHAGY

DEMET AÇIKGÖZ

M.Sc. THESIS

DEPARTMENT OF MEDICAL BIOTECHNOLOGY

SUPERVISOR
Assoc. Prof. Devrim Öz Arslan

ISTANBUL-2022

ACIBADEM MEHMET ALI AYDINLAR UNIVERSITY
INSTITUTE OF HEALTH SCIENCES

UNRAVELING NEW BINDING PARTNERS OF ATG3 IN AUTOPHAGY AND MITOPHAGY

DEMET AÇIKGÖZ

M.Sc. THESIS

DEPARTMENT OF MEDICAL BIOTECHNOLOGY

SUPERVISOR
Assoc. Prof. Devrim Öz Arslan

ISTANBUL-2022

Department:	MEDICAL BIOTECHNOLOGY
Program:	MEDICAL BIOTECHNOLOGY
Thesis Title:	UNRAVELING NEW BINDING PARTNERS OF ATG3 IN AUTOPHAGY AND MITOPHAGY
Student's Name and Surname:	DEMET AÇIKGÖZ
Date of Defence:	26/01/2022

This is to certify that I have examined this copy of master thesis. I have found that she prepared after fulfilling the specified requirements in the associated legislation before the final examining committee whose signatures are below.

DECLARATION

I declare that this thesis work is my own work, I had no unethical behavior at any stages from the planning to the writing of the thesis, I obtained all the information in this thesis in accordance with academic and ethical rules, I cited all the information and comments that were not obtained with this thesis work, and I provided resources in the list of references. I also declare that there was no violation of any patents and copyrights during the study and writing of this thesis.

04/01/2022
Demet AÇIKGÖZ

PREFACE AND ACKNOWLEDGEMENT

First and foremost, I would like to give my biggest appreciation to my supervisor Assoc. Prof. Devrim ÖZ ARSLAN for her time, patience, guidance, and all experiences that share with me generously in her laboratory. I would like to thank Assoc. Prof. Zeynep Aslıhan DURER for her time, help, advice, the contribution to my knowledge during this thesis study. I am also thankful to Prof. Beki KAN for her teachings and suggestions in this project.

My gratitude goes out to all my colleagues; Simge ŞENAY, Hande KASAP, Hande İpek YETKE, and Tuğçe DEMİR who supported and helped me through this project. My appreciation also goes to Görkem GÜN and other members of Acibadem Mehmet Ali Aydınlar University Research Laboratory Center.

I would like to thank my father for his infinite faith and support for my study and this thesis. I am kindly grateful to my best friends; Gizem KEÇELOĞLU, Büşra KÖSE, Kübra Nilüfer AKA, and Buse KESKİN for their support and wise opinions and helped me get through good times and the bad.

I would also like to thank Acibadem Mehmet Ali Aydinlar University for providing laboratory facilities and to Scientific and Technological Research Council of Turkey (TUBITAK) for their financial support.

I would like to thank Merve ÖZTUĞ KILINÇ for her work and collaboration to perform LC-MS/MS analysis and Emel TİMUÇİN and Süleyman BOZKURT for their support and help with bioinformatic analysis in this thesis.

This study was supported by TUBITAK 3001 project (217Z213); I was supported as a fellow from 2018 to 2020.

TABLE OF CONTENTS

LIST OF ABBREVIATIONS

ATG	Autophagy Related Genes
ATG3	Autophagy Related Protein 3
ATP	Adenosine triphosphate
CCCP	Carbonyl Cyanide 3-chlorophenylhydrazone
CMA	Chaperon Mediated Autophagy
DMSO	Dimethyl Sulphoxide
ΔΨm	Mitochondrial membrane potential
DTT	DL-Dithiothreitol
EDTA	Ethylediaminetetraacedic acid
ER	Endoplasmic reticulum
FBS	Fetal Bovine Serum
HSS	High Speed Supernatant
IDP	Intrinsically Disordered Proteins
IDPR	Intrinsically Disordered Protein Regions
IMM	Inner Mitochondrial Membrane
LSS	Low Speed Supernatant
µl	Microlitre
µg	Microgram
mTORC	mTOR complex
MAP1LC3	Microtubule-Associated 1A/1B LC3
mins	Minutes
ml	Milliliter
mM	Millimolar
mTORC1	Mammalian Target of Rapamycin Complex 1
MTT	3-(4,5-Dimethylethiazol-2-yl)-2,5-Diphenyltetrazolium Bromide
OMM	Outer Mitochondrial Membrane
P13K	Phosphatidylinositol-3-kinase
PARKIN	PINK1 and E3-Ubiqutin Ligase
PAS	Phagophore Assembly Site
PBS	Phosphate Buffer Saline

PE	Phosphatidylethanolamine
PI	Phosphatidylinositol
PI3KC3	Class 3 Phosphatidylinositol 3-Kinase
PINK1	PTEN Induced Putative Kinase Protein
PMSF	Phenylmethanesulfonylfluoride
PVDF	Polyvinylide Fluoride
RIPA	Radioimmunoprecipitation assay
SDS	Sodium Dodecylsulfate
ULK 1/2	Unc–51 Like Kinase Family 1/2
UPR	Unfolded Protein Response

LIST OF FIGURES

LIST OF TABLES

ÖZET

ATG3 PROTEİNİN ÖZGÜN ETKİLEŞİM PARTNERLERİNİN ARAŞTIRILMASI

Otofaji, hücre içinde hasar görmüş organellerin, yanlış katlanmış protein kümeleri gibi kalıntıların otofagozom içine alınarak daha sonra bu otofagozomun lizozom ile birleşmesi sonucunda parçalanması ile hücresel yapı taşlarının yeniden kazanılmasını sağlayan önemli bir geri dönüşüm mekanizmasıdır. Otofagozom oluşumu evrimsel olarak korunmuş ve günümüze kadar literatürde tanımlanmış 40'tan fazla çeşidi bulunan ATG proteinleri ile ilişkilendirilmiş bir süreçtir. Bu proteinler arasında yer alan ATG3 proteini otofagozom oluşumunda ve uzamasında kritik bir role sahiptir. ATG3'ün yapısal ve hücresel özellikleri göz önüne alındığında hücre içinde otofajiden bağımsız rolleri de olabileceği ifade edilmektedir. Bu bilgiler ışığı altında, bu çalışmanın amacı, ATG3 proteinin otofaji ve seçiçi otofaji türü olan mitofaji uyaranları varlığında ve yokluğunda farklı yolaklardaki etkileşim partnerlerinin belirlenmesidir. mEmerald-ATG3-N-18 plazmidi ile transfekte edilen insan hepatoma hücre hattı (Hep3B) otofaji (TORIN 1) ve mitofajiye (CCCP) indüklendi. Bu hücrelerden ATG3-GFP füzyon proteinleri ve partnerleri GFP temelli affinite çöktürme yöntemi kullanılarak çöktürüldü ve LC-MS/MS ile analiz edildi. LC-MS/MS verileri "Protein Discoverer (Thermo Scientific)" yazılımı ile protein ifadesindeki farklılıklar tespit edilerek biyoinformatik analizler yapıldı. Kontrol, otofaji ve mitofaji ile indüklenen hücrelerde Reactome yolak analizi, STRING etkileşim yolak analizleri kullanılarak biyoinformatik analizler yapıldı. Bu analizler ATG3'ün; ATG5, ATG7, ATG12, ATG16L1, GABARAPL2, LC3B gibi bilinen partnerlerinin yanı sıra hücresel stress yanıtında görev alan bilinmeyen partnerler ile güçlü olarak etkileştiğini gösterdi.

Anahtar Sözcükler: ATG3, Otofaji, Mitofaji, Afinite çöktürme, Partner protein, LC-MS/MS

ABSTRACT

UNRAVELING NEW BINDING PARTNERS OF ATG3 IN AUTOPHAGY AND MITOPHAGY

Autophagy is a cellular process whereby damaged proteins, protein complexes, and organelles are engulfed by autophagosomes and then fused with lysosomes for degradation. The cargo is recycled for the retrieval of macromolecular building blocks. One of the key events in this process is autophagosome formation. During the formation of autophagosomes, more than 40 evolutionarily conserved autophagy-related proteins (ATG) are involved. ATG3 has a crucial role in autophagosome formation and elongation. Considering the structural and cellular functions of ATG3, it is proposed to have additional roles independent of autophagy. In light of this knowledge, this study aims to investigate novel interaction partners of ATG3 in the presence and absence of autophagy and mitophagy modulators. Human hepatoma cell lines, (Hep3B cells) were transfected with mEmerald-ATG3-N-18 and then treated with Torin 1 and CCCP for induction of autophagy and mitophagy, respectively. ATG3-GFP and its complexes were pulled down using ChromoTek GFP-Trap® agarose beads and analyzed with LC-MS/MS. ATG3-GFP fusion proteins and their partners were immunoprecipitated from transfected cells and analyzed with LC-MS/MS to compare control, autophagy, and mitophagy induced groups. LC-MS/MS data were analyzed using the "Protein Discoverer (Thermo Scientific)" software for assessing protein expression differences. Reactome pathway analysis and STRING analysis indicated that ATG3 displays interaction with known partners, ATG5, ATG7, ATG12, ATG16L1, GABARAPL2, LC3B, as well as unknown partners involved in cellular stress response.

Keywords: ATG3, Autophagy, Mitophagy, Pull-down, Binding Partner, LC-MS/MS

1. INTRODUCTION AND AIM

Autophagy is a cellular stress response to starvation, growth factor depletion, hypoxia, and infection. Several studies revealed how the regulation of autophagy affects signaling pathways and diverse cellular mechanisms. The essential role of autophagy is providing nutrients for cell survival functions during starvation and other stress factors. Macroautophagy is a unique and non-selective autophagy process regarding *de novo* autophagosomes morphological features (1). Autophagosome formation begins with the initiation of a phagophore, a site called phagophore assembly site (PAS) in yeast while in mammals initiation step starts at multiple sites. Autophagosome engulfs cargos and is fused with lysosome for degradation. Following this event, recycled molecular building blocks are released into the cytosol.

Autophagy can also be used for specific degradation, which is called selective autophagy such as damaged mitochondria degradation via mitophagy. Mitochondria is a dynamic organelle that moves steadily to make new connections and divisions. Mitochondrial dynamics involve two important events that are named fusion and fission that are crucial for mitochondrial quality control (2). The preliminary step of mitophagy is to detect damaged mitochondria that should be eliminated from healthy ones (3). This process starts with a double-membrane structure formation called the autophagosome.

ATG proteins are autophagy-related proteins that are responsible for autophagosome formation. There are approximately 40 ATG proteins that have been defined in the literature (4). ATG3 is an E2-like enzyme that helps phosphatidylethanolamine (PE) conjugation to ATG8 (mammalian LC3) protein (5). ATG3 also plays a crucial role in the mitochondrial quality control process and mitophagy pathway. In addition, ATG3 is upregulated in several types of tumors. Therefore, understanding ATG3 function may help to navigate the different cellular processes and pathologies affected by this protein.

This study aims to investigate the novel partners of ATG3 during autophagy and mitophagy. Identifying new binding partners will help explain diverse cellular processes where ATG3 participates. It may also help clarify the role of ATG3 during mitophagy and autophagy. For this purpose, autophagy and mitophagy were induced in hepatocytes transfected with GFP-tagged ATG3 plasmids. Once autophagy and mitophagy were induced, GFP-tagged ATG3 proteins were pulled down by using affinity purification methods. Pull-down samples were analyzed with LC-MS/MS mass spectrometry to identify ATG3 binding partners. Then, bioinformatics tools were used to indicate ATG3 interactions and pathways analyzed.

Definition of new interaction partners for ATG3 during mitophagy and autophagy will provide a better understanding of the role of ATG3 in different cellular processes. As a future aspect, these findings will enable the design of molecules targeted to disorders where autophagy and mitophagy may play a vital role, such as metabolic diseases, ischemic heart disease, and neurodegeneration.

2. BACKGROUND

2.1 Autophagy

Autophagy is a highly conserved process in all eukaryotes and was mentioned first by Christian de Duve in 1963. Autophagy terminologically is derived from Greek words meaning “auto”-self and “phagy”-eating. The degradation process of all cell components such as organelles, misfolded proteins, and macromolecules is accomplished by autophagy (6). Autophagy is a recycling process that provides energy for the cell under stress conditions such as nutrient depletion, hypoxia, or chemotherapeutic drugs (7–9). Understanding these pathways is crucial because defects in the selective autophagy of various organelles have been associated with conditions including inflammatory diseases, metabolic diseases, cancer, neurodegeneration (10), and aging (11, 12).

There are three main types of autophagy: macroautophagy, microautophagy, and chaperone-mediated autophagy (Figure 1). All three types of autophagy involve the transportation of cytosolic components to the lysosome for recycling and degradation. Microautophagy is simply defined as cell components that are directly captured by lysosome and the mechanism is still not revealed in detail (1). Chaperone-mediated autophagy (CMA) differs from microautophagy and macroautophagy by not initiating from membranous structures. The cargo is recognized by a chaperone protein known as HSC70/HSPA8 and then gets transported to the lysosome (13). CMA is based on a pentapeptide motif knits known as KFERQ (14). It is a highly specialized process that targets peptide sequences. The cargo with the KFERQ motif interacts with the chaperones directly, targeting them to the lysosome membrane through lysosomal-associated membrane protein 2A (LAMP2A) (15). Macroautophagy is the main autophagic pathway. The process is characterized by the formation of an intermediary double-membrane vesicle, autophagosome, which engulfs cytoplasmic components and is transported to the lysosome. It is a highly unique process and differs from microautophagy and CMA where the autophagosomes membrane does not bud from any organelles or membranous structures in the cytosol and is therefore named *de novo* form (1).

Following macroautophagy initiation, phagosome formation begins at the phagophore assembly site (PAS) in yeast while in mammals it is initiated at multiple sites (16). Studies suggest that the omegasome which is related to endoplasmic reticulum structure is the initiation site in mammals (17).

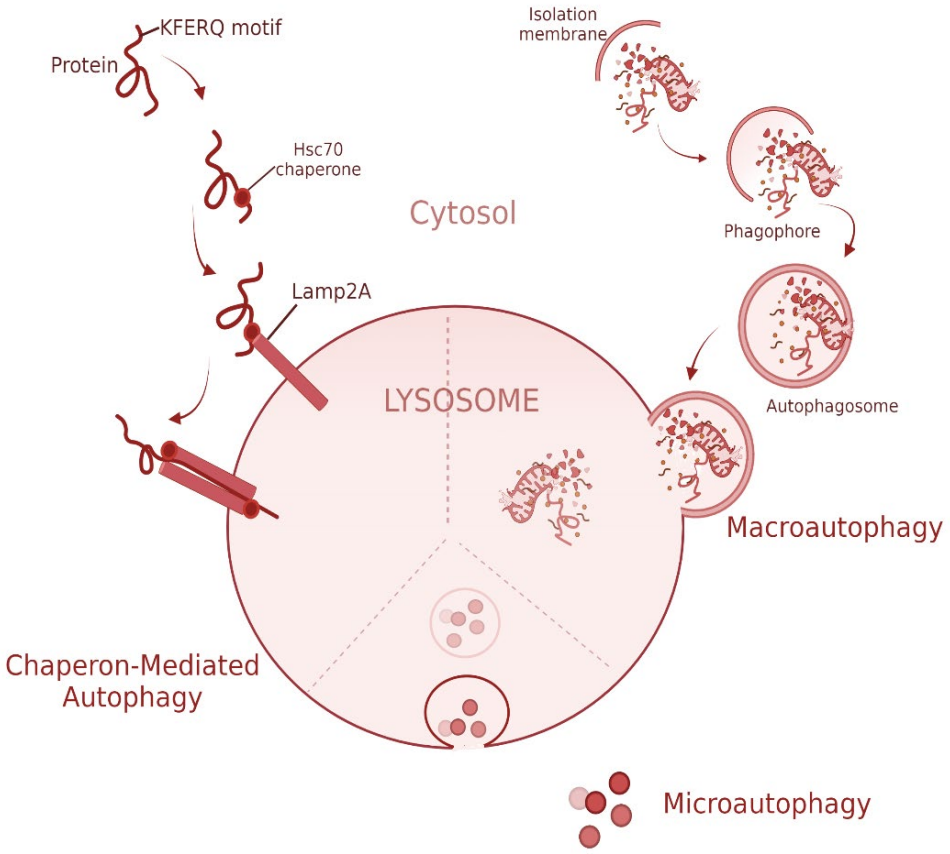

Figure 1. Three types of autophagy.

2.2 Autophagosome Formation

The formation of autophagosomes is a crucial step for autophagy machinery. Proteins which are involved in the regulation of autophagy machinery and autophagosome formation are called autophagy-related proteins (ATG) and were first identified in yeast. To date, 40 ATG proteins have been defined and 16 of them are "core" ATG genes that contribute both to selective and non-selective autophagy. The

discovery of ATG proteins provided an understanding of the relationship between autophagy and intracellular trafficking machinery.

Autophagosome formation has four main steps: initiation, elongation, lysosome fusion, and degradation (Figure 2). Initiation of phagophore may occur in two ways. One complex consists of the class III PI3K/Vps34, ATG6/Beclin1, ATG14, and Vps15/p150 and the other complex is serine/threonine kinase Atg1/ULK1 which is a positive regulator of formation. One of the well-known signaling complexes for autophagy initiation is the ULK-1 complex. It consists of ULK-1 and ULK-2 kinases and regulatory proteins such as ATG13, FIP200, and ATG101 (18–20). Under normal conditions, the mammalian target of rapamycin (mTOR) complex 1 binds the ULK-1 complex, and autophagy is inhibited. mTORC1 is known as a regulator responsible for cell growth and metabolism. Starvation blocks mTORC1 activity and releases the ULK-1 and ULK-2 proteins under stress conditions, activating autophagy. When ULK complexes are activated the class III PI3 kinase complex, another key regulator of the autophagy mechanism, is activated. The PI3KC3 is involved in autophagy initiation and is composed of VPS34 (bearing the enzymatic activity) VPS15, Beclin1, and ATG14L (21). Targeting of VPS34 leads to the synthesis of PI3P and involves specific recruitment of binding proteins such as DFCP1 or WIPIs (22, 23).

Autophagosome initiation leads to nucleation or elongation steps (Figure 2). Primary double-membrane sequestration which is called phagophore starts to expand after initiation (24). Following elongation, the membrane is curved while the phagophore size is based on the type and size of cargo (25). The elongation and closure of the isolation membrane are managed by two different ubiquitin-like conjugation systems. The ATG12-ATG5-ATG16 complex is the first one in which E1-like ATG7 (26) and E2-like Atg10 (27) conjugate the ubiquitin-like ATG12 to ATG5. ATG12 and ATG5 complex connects with ATG16 to form the ATG5-ATG12-ATG16 complex (28). WIPI2 protein has a unique role in targeting the ATG5-ATG12-ATG16L1 complex to the PI3P-positive membrane and other ATG proteins such as ATG3, ATG7, and ATG10 which are highly important proteins for LC3 lipidation (24, 25). The second ubiquitin-like conjugation system is phosphatidylethanolamine (PE)

lipid assembly to ATG8 in yeast (LC3 in mammals). Firstly, ATG8 is activated by ATG4 (29) and then ATG8 is bound to PE which is processed by ATG7 and E2-like ATG3 enzymes. LC3 lipidation is a positive signal for autophagosome formation (30). The molecular sequence of initiation is important for the nucleation of phagophores even though some of the ATG proteins are required to act as scaffolds for membrane maturation. Autophagosome is formed when the phagophore is closed. Autophagosomes may contain non-specific cargo or specific cytoplasm portions and cargoes that are recognized by autophagy receptors (31, 32).

Autophagosome maturation completes after lysosome fusion. At this stage, lysosomal enzymes hydrolyze cytosolic compartments (Figure 2). Many proteins are identified for autophagosomal maturation such as Rab small GTPases, SNAREs, and VPS proteins (33). SNARE proteins including Syntaxin-17 (STX17), SNAP29, and VAMP8 are responsible for autophagosome fusion with the lysosome (34). Autophagosomes have also been shown to be directed to the plasma membrane for specific secretion (35) or to fuse with endosomal compartments to generate an intermediate and transient organelle called amphisome (36, 37).

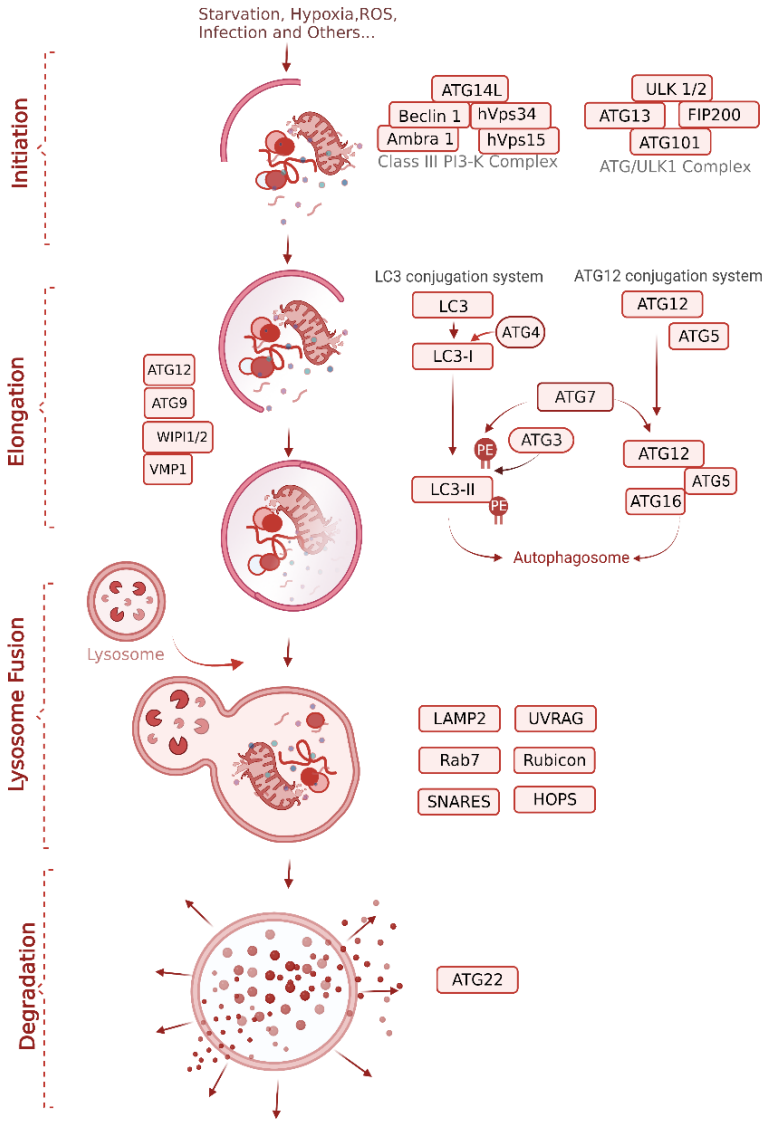

Figure 2. Autophagosome formation and related proteins.

Early studies revealed that autophagosome accumulation may cause diverse neurodegenerative diseases including Alzheimer's disease, Parkinson's disease, and Huntington's disease (38, 39). In addition, autophagy has been implicated in many other pathological conditions. The reason for this may be either the failure of autophagosome fusion with lysosomes or the aggregation of misfolded proteins.

Autophagy regulation is closely associated with signaling pathways. Many tumor suppressor genes engage with upstream inhibition of TOR signaling, induce autophagy, and conversely, oncogene products such as class I PI3K and Akt activation can cause

inhibition of autophagy (40, 41). Somehow, activation of autophagy does not always have a positive effect. For example, the tumor cells can survive under hypoxic conditions using autophagy. On the other hand, if the autophagosome and lysosome fusion is disrupted, activation of autophagy may lead to the accumulation of cellular protein aggregates that may cause pathologies such as Parkinson's disease, and other neurodegenerative disorders (42).

2.3 Intrinsically Disordered Proteins in Autophagy

Proteins, which fail to form a unique regular three-dimensional (3D) structure in their active state, are defined as intrinsically disordered proteins (IDP). In some cases, specific regions called intrinsically disordered protein regions (IDPR) in proteins are flexible and have formed a dynamic ensemble in an aqueous solution (43). IDP's classification has three different subclasses; completely unstructured proteins, pre-molten globule-like, and molten globule-like proteins, and hybrid proteins that have ordered and disordered regions at the same time.

The conformational flexibility of IDPs provide many biological advantages to them over globular proteins (42–44). The structural flexibility of IDPs improves interaction speed and limits restrictions, enabling the IDPs to interact with larger surfaces. The disordered region of the IDPs can bind several partners. IDPs and IDRs can have important roles in post-translational modifications where the flexible region provides a cascade-type of binding. IDPs are usually involved in cell signaling and regulation pathways (43, 45, 46).

Table 1. Intrinsically Disordered Proteins in Autophagy

Autophagy Initiation Signaling Complex	ULK1
	ULK2
	ATG13
	RB1CC1
	PIK3R4

Table 2. Intrinsically Disordered Proteins in Autophagy (Continue)

Autophagy Initiation Signaling Complex	BCN1
	ATG14
	AMBRA1
	UVRAG
	VMP1
	PIK3C3
Autophagosome Expansion Complex	ATG16L1
	ATG12
	ATG3
	ATG4D
Autophagosome Maturation Complex	ATG9A
	WIPI1
	ATG2A
	SNX18
Autophagy Targeting Proteins	NBR1
	SQSTM1
	SMURF1
Autophagy Regulation	BNIP3L
	BNIP3
	BCL2
	BCL2L1
	KIAA0226
	CLN3
	GOPC
	TMEM74
	PINK1
	HMGB1
	EXOC8
	HDAC6

IDRs may be beneficial in three ways for macromolecular interactions: 1) low binding affinity causes specific interactions that can be reversible, 2) flexible regions contribute conformational advantage to change several proteins, expand interaction surfaces and increase interaction speed, 3) IDRs different domains may bind different partners and this is highly important in signaling process (47).

Previous bioinformatic analyses showed the presence of IDRs in key autophagy proteins (Table *1*). Most of IDRs' biological functions have not been elucidated yet (48). The understanding of the IDRs role and mechanism in autophagy will shed light on the mechanism of related cellular pathways and may lead to the identification of new therapeutic targets in autophagy.

IDRs are mostly observed in the variable region of ATG proteins. Since IDRs show low conservation across species, their identification is difficult (49, 50). Since IDPs are critical in protein-protein interactions or signaling cascades, many recent studies are focused on identifying interaction partners of IDPs (51). In addition, 50% of ATG proteins in yeast are described as IDPs (52). Therefore, clarifying the role of IDPs in ATG protein structure will help better understand the mechanism of autophagy.

2.4 Ubiquitin-like Conjugating Enzyme ATG3

Autophagosomes formation and maturation are the critical steps during autophagy (39). During autophagosome maturation, a specific E1-E2-E3 enzymatic cascade contributes to the conjugation of phosphatidylethanolamine (PE) to ATG8-family ubiquitin-like proteins. This process is catalyzed by ATG3, E2 like enzyme, and an additional substrate for ATG12 conjugation (Figure 3).

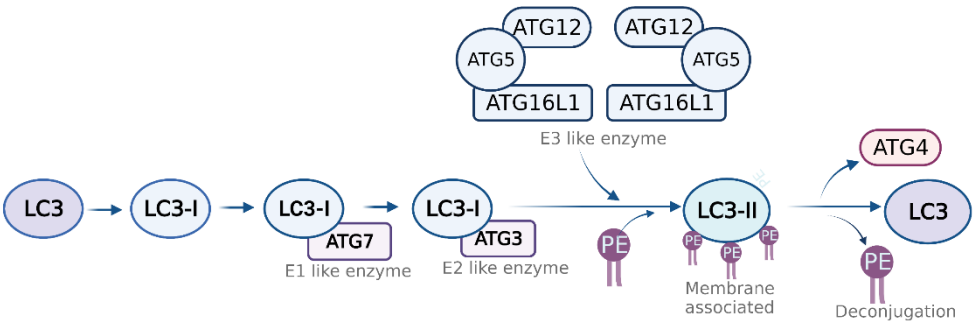

Figure 3. E1-E2-E3 enzymatic cascade and LC3-PE conjugation.

ATG3's crystal structure in *Saccharomyces cerevisiae* at 2.5-Å resolution shows that one-third of the sequence of ATG3 is missing in the crystal structure (Figure 4) (53). The protein structure of ATG3 contains α and β folds and its core region is topologically like canonical E2 enzymes. ATG3 is classified as an intrinsically disordered protein since it has a significant amount of disordered regions similar to an E2-like enzyme (54). E2 enzymes have four subclasses (55). Class I has a very preserved E2 core and has no extension; classes II and III have carboxyl- and amino-terminal extensions, (56, 57), and class IV has both E2 core and extensions (58). Even though ATG3 is topologically similar to the E2 core region, the structure has many differences. ATG3 has a distinctive protein structure including an N-terminal membrane-binding helix (N), an intrinsically disordered flexible region (FR) a handle region (HR), and a flexible C-terminal tail (C) (Figure 4A) (56). ATG3 has no carboxyl-terminal-helices and instead has two large insertions, which are defined as HR and FR in the core region. *In vitro* and *in vivo* studies claimed that these insertions may have a crucial role in ATG8-PE conjugation and that FR and HR regions are both responsible for ATG7 and ATG8 binding (Figure 4).

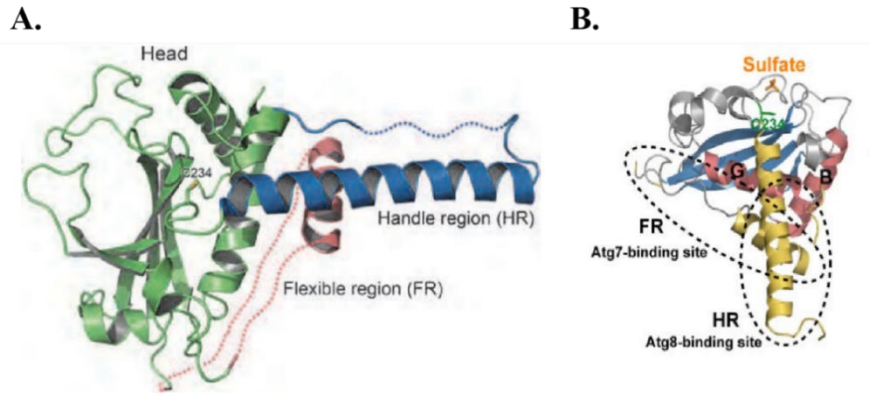

Figure 4. Crystal structure of ATG3.

((A) Crystal structure of ATG3. Handle region (HR) and flexible region (FR) are represented in blue and red respectively. (B) ATG7 and ATG8 binding sites of ATG3 crystal structure (59).)

Ubiquitin interacts with its target proteins on the C-terminus site and this process occurs through a specific protease targeting a glycine residue at the C terminus site. Then this glycine residue at the C terminus is activated by an E1-like enzyme to deliver the E2 enzyme. This brings an E3 enzyme to ubiquitinate the target protein (60). Mammalian LC3 protein (homologous Atg8 in yeast) is a protein that is a ubiquitin-like modifier. However, its target is a phospholipid: phosphatidylethanolamine (PE) (61). This conjugation process has similar properties to ubiquitination (62). ATG8's carboxyl-terminal arginine is activated by ATG4 which is a cysteine protease (63, 64). When autophagosome formation occurs, LC3 precursor proteins are cleaved into LC3-I form at the site of Gly120 by ATG4B protease. At this step, LC3-I is activated by the E1-like enzyme, ATG7, and then transported to the E2-like enzyme, ATG3. Next, this LC3-I-ATG3 complex binds the E3-like ligase ATG12-ATG5 in order to initiate the conjugation with PE. This conjugation is highly conserved in autophagosome formation (65). However, LC3 lipidation can occur independently of ATG5-ATG7 conjugation during the non-canonical process yet there is not any evidence that ATG3 deficient cells can convert LC3-I to LC3-II (66, 67). ATG3 functions have not been studied extensively in mitochondrial homeostasis, tumor progression, and viral infection clearance (68–70). Although ATG12 and ATG3 both play a critical role in autophagosome formation, the knockdown of ATG12-ATG3 complexes in cells doesn't have any effect on starvation-induced autophagy. However, nutrient-rich conditions in the absence of ATG12-ATG3 can demonstrate increased autophagosome

numbers (68). ATG3's known interaction partners are ATG7, ATG8, ATG12, and phospholipids. A novel study has shown that the role of ATG3 in autophagosome formation is more complex than recent findings so far because ATG3 may also act as a tethering factor during autophagosome elongation (71).

The effect of autophagy on cancer is a complex issue. Since autophagy is a pro-survival mechanism, it provides recycled nutrients and helps clear the damaged organelles of cancer cells resistant to chemotherapy radiation and immunotherapy (72). ATG3 expression can vary in many types of cancer tissues. Previous experiments revealed that knockdown of ATG3 inhibited proliferation and invasion of colon cancer cells (73). A further study claimed that ATG3 overexpression can induce autophagy and enhance bortezomib drug sensitivity in SKM-1 cells (72). It is suggested that the low levels of ATG3 expression are observed in leukemia and, therefore, the regulation of autophagic activity may be an advantage in differentiation therapies (74).

Current evidence shows that ATG3 is a crucial regulator of cell survival and death. ATG16 deficient mice can survive while ATG3 deficient mice will die within a day. Experiments with ATG3 deficient MEF cells implied that ATG3 is also important for cell differentiation (75–77). ATG3 is also a direct target of caspase-8 and plays important role in autophagy regulation during cell death and survival (56). ATG3 functions during DNA damage, independent of autophagy. The inhibition of ATG3 degradation could cause DNA damage-induced mitotic catastrophe through BCL2 interaction (78).

Furthermore, ATG3 can restrain autophagy-induced apoptosis in inactivated Sedai virus (HVJ-E) treated cells (79). The downregulation of ATG3 expression was reported to cause limited embryonic stem cell renewal, differentiation, and pluripotency (76). ATG3 is also related to plant growth. For example, it may contribute to the tuber apical dominance of potatoes (80). ATG3 also plays an important role to regulate immunity in plants against tobacco mosaic virus (TMV) (81). Although autophagy-independent functions of ATG3 remain limited, investigating post-translational modifications might help to discover novel functions of ATG3.

2.5 Role of ATG3 in Mitophagy

Mitochondria are the energy source of cells functioning in ATP synthesis, calcium buffering, and the regulation of apoptosis (82). Mitophagy is a selective autophagic process for the removal of damaged mitochondria and was first mentioned by Lemasters in 2005 (83). Mitochondria have a double-membranous structure called inner mitochondrial membrane (IMM) and outer mitochondrial membrane (OMM) (84). The generation of adenosine triphosphate (ATP) and reactive oxygen species (ROS) occurs in IMM. The mitochondrial electron transport chain (ETC) system has four complexes (I-IV). ATP generation from ADP and Pi occurs by ATP synthase which uses the electrochemical potential energy (85, 86). Moreover, mitochondria regulate intracellular calcium transport and ion levels by providing ATP for calcium transporting proteins and calcium signaling (86).

Mitochondrial dysfunction leads to depolarized mitochondrial membrane potential ($\Delta\Psi m$), increased ROS levels, and an increase in mitophagy (87). Each cell has different bioenergetic demands, and cells can regulate mitochondrial homeostasis through either biogenesis and degradation or dynamic fusion and fission events (88). Mitochondria undergo continuous cycles of fission and fusion processes for the maintenance of overall mitochondrial structure and function. Mitochondrial fragmentation reveals an imbalance in fission and fusion and disruption of the ATG12-ATG3 complex which promotes reduced mitochondrial fusion activity (89). It was shown that the loss of ATG3 in Toxoplasma gondii caused crucial mitochondrial fragmentation (90). ATG3 deficiency caused increased glycolysis and mitochondrial metabolism activity. Also, loss of ATG3 in adipocytes led to dysfunctional mitochondria accumulation and increased lipid peroxidation, systemic insulin resistance, and adipose tissue inflammation (91).

Mitochondrial remodeling and reprogramming are regulated by ATG3-dependent autophagy. ATG3 deletion can cause mitochondrial accumulation and it is claimed that ATG3-dependent autophagy regulates both mitochondrial quality and quantity at the same time (92). As in an alternative perspective, ATG12-ATG3 conjugation may

change ATG3's substrate specificity and change enzymatic activity or promote new protein-protein interactions (93).

3. MATERIALS AND METHODS

3.1 Materials

Table 3. List of Products and Suppliers

0% Fat Skim milk	Regilait
0.25% Trypsin-EDTA, phenol RED	Gibco
2-mercaptoethanol	Sigma Aldrich
40% Acrylamide/Bis-acrylamide	Serva
Acetic Acid	Sigma Aldrich
Anti-ATG5 (N-terminal) antibody produced in rabbit	Sigma Aldrich
Anti-ATG7 antibody produced in rabbit	Sigma Aldrich
Amersham Hybond P 0.2 PVDF membrane	GE Healthcare
Amersham Protran 0.2 NC membrane	GE Healthcare
Ammonium persulphate	GE Healthcare
Bovine Serum Albumin (BSA) Fraction V	Sigma Aldrich
Bradford Reagent, 5x	Serva
Brillant Blue G	Sigma Aldrich
ChromoTek GFP-Trap™	ChoromoTek
Carbonyl cyanide 3-cholorophenylhydrazone (CCCP)	Sigma Aldrich
Cell Proliferation Kit	Roche
Dimethyl sulphoxide (DMSO) Hybri-Max	Sigma Aldrich
DMEM, high glucose, non-pyruvate	Gibco
DTT	Applichem
DUALL KONTES™ Tissue Grinder	Fisher Scientific
EDTA-free protease inhibitor cocktail	Roche
Ethanol	Sigma Aldrich
Ethylenediaminetetraacedic acid (EDTA)	Sigma Aldrich

Table 2. List of Products and Suppliers (continue)

Glycerol	Sigma Aldrich
Glycine	Serva
HEPES	Sigma Aldrich
HI Fetal Bovine Serum	Gibco
Hydrochloric acid	Sigma Aldrich
Igepal CA-630	Sigma Aldrich
L-Glutamine	Gibco
Lipofectamine 3000 Transfection Kit	Invitrogen
Methanol	Sigma Aldrich
Mouse monoclonal anti-B-Actin Antibody (AC-74)	Sigma Aldrich
Opti-MEM	Gibco
PageRuler™ Plus Prestained Protein Ladder 10 to 250kDa	ThermoFisher Scientific
Pei-MAX	Polysciences
Penicillin-Streptomycin	Gibco
Peroxidase affinipure goat anti-mouse IgG(H+L)	Jackson Immoresearch
Peroxidase affinipure goat anti-rabbit IgG(H+L)	Jackson Immoresearch
Phenylmethanesulfonyl (PMSF)	Applichem
Phosphate Buffer Saline (PBS), 1X	Gibco
Ponceau S	Sigma Aldrich
Potassium Chloride	Sigma Aldrich
Potassium dihydrogen phosphate	Sigma Aldrich
Rabbit monoclonal anti-Cox IV (3E11)	Cell Signaling Technology
Rabbit polyclonal anti-LC3B	Sigma Aldrich
Rabbit polyclonal anti-p62/SQSTM1	Novus Biologicals
Rabbit polyclonal PINK1 Antibody	Novus

Table 2. List of Products and Suppliers (continue)

SDS	Sigma Aldrich
Sodium Azide	Sigma Aldrich
Sodium Chloride	Sigma Aldrich
Sodium Fluoride	Sigma Aldrich
Sodium hydroxide	Merck
Sodium orthovanadate	Sigma Aldrich
Sodium phosphate dibasic dodecahydrate	Sigma Aldrich
SuperSignal West Pico Chemiluminescent Substrate	ThermoFisher Scientific
TEMED	Sigma Aldrich
Triton X-100	Sigma Aldrich
Trizma Base	Sigma Aldrich
Trizma Base for Electrophoresis	Serva
Trypan Blue	Sigma Aldrich
Tween 20	Sigma Aldrich
Zeba™ Spin Desalting Column	Thermo Fisher Scientific
Zymo Pure Midi Prep Kit	ZymoPure
Western Blotting filter extra-thick paper	ThermoFisher Scientific

Table 4. List of Equipment

-20ºC freezer	Kirsch
-80ºC freezer	GLF
4ºC fridge	Kirsch
Biosafety cabinet	ThermoFisher Scientific
Cell Culture Incubator	ESCO CCL-170B-8
ChemiDoc MP Imaging System	BioRad
Environmental Shaker/Incubator	ESCO
Flow Cytometer	BD FACSVerse

Table 5. List of Equipment (continue)

Inverted Microscope	Zeiss
Micro Centrifuge	ThermoFisher Scientific
Mini Centrifuge	Biosan
Nitrogen Tank	Thermo 30 Thermo Scientific
Plate Reader	BioTek
Trans-Blot turbo Tranfer system	BioRad
Varioskan flash	ThermoFisher Scientific
Ventilated microcentrifuge	ThermoFisher Scientific
Water Bath	St 30 Nüve

3.1.1 Preparation of chemicals, solutions, and buffers

CCCP (20mM)

0.005g of CCCP was dissolved in 1220 µl of DMSO to prepare 20 mM main stocks. The stock solution was filtered with a 0.22 um filter and stored at -80°C.

Torin 1 (1mM)

2,2 mg Torin 1 was dissolved in 3620 µl DMSO and aliquoted and stored at -80ºC.

Protease Inhibitor (PI) (25x)

Roche cOmplete EDTA-free protease inhibitor cocktail was dissolved in 2 ml of ddH2O to obtain 25X PI. PI solution was stored at -20°C. During protein isolation, PI was diluted with RIPA buffer to 1X concentration.

Table 6. 15% Polyacrylamide Separating Gel (1x)

% 40 Acrylamide/Bis-acrylamide	2.5 ml
1.5M Tris (pH:8.8)	1.25 ml
50% Glycerol	375 µl
ddH_2O	875 µl
10% APS	50 µl
TEMED	5 µl

Table 7. 12% Polyacrylamide Separating Gel (1x)

30% Acrylamide/Bisacrylamide	2 ml
1.5 M Tris (pH 8.8)	1.25 ml
50% Glycerol	375 µl
ddH2O	1375 µl
TEMED	5 µl
10% APS	50 µl

Table 8. 4% Polyacrylamide Stacking Gel (1x)

30% Acrylamide/Bisacrylamide	325 µl
1 M Tris (pH 6.8)	625 µl
20% SDS	12.5 µl
ddH2O	1512 µl
10% APS	12.5 µl
TEMED	5 µl

Tris-Glycine running buffer (pH 7.5-8.0), 10x

25 mM Tris

1.92 M Glycine

1% SDS

1X running buffer is diluted from 10X stock with ddH2O

Bjerrum Schafer-Nielsen Transfer buffer, 10x

48 mM Tris

39 mM Glycine

20% methanol

1X transfer buffer is diluted from 10X stock with ddH2O

PBS (pH 7.4), 10x

30 mM KCl

1.37 M NaCl

35 mM KH2PO4

100 mM Na2HPO4.12H2O

1X PBS is diluted from 10X stock with ddH2O

RIPA lysis buffer, 1x

50 mM Tris-HCl (pH 7.4)

150 mM NaCl

1 mM NaF

1 mM EDTA

1 mM Na3VO4

0.5 % Igepal CA-630

0.5 % Triton X-100

1 mM DTT

0.5 mM PMSF in EtOH

Skimmed Milk, 5 %

1X PBS-T is used to prepare 5 % (w/v) skimmed milk

PBST, 1X

1X PBS

% 1 Tween-20

BSA for primary antibodies, 5 %

5 % (w/v) Fraction V BSA

1X PBS

0.02 % NaAzide

Laemmli Sample Buffer, 5X

250mM Tris-HCl (pH 6.8)

5 % SDS

43.5 % Glycerol

0.5 % Bromophenol Blue

Ponceau S

0.1 % (w/v) Ponceau S

5 % Acetic acid

Hepes 50 Buffer 100ml

50 mM HEPES ph:7.5

100mM NaCI

0,5mM EDTA

1mM NaF

1mM Sodium orthovanadate (Na3VO4)

Hepes buffer was divided into 50ml tubes after preparation. The prepared buffer was stored at -80°C.

Lysis Stock Buffer

Hepes50 Buffer 50ml

0.25% Triton

0.25% Glycerol

The prepared buffer was stored at -80°C.

100X Protease Inhibitor, 1mM PMSF, and 10mM β-mercaptoethanol were added freshly to make the Lysis Working Stock Buffer.

Wash Stock Buffer

Hepes50 Buffer 50ml

0.25% Tween20

The prepared buffer was stored at -80°C.

1mM PMSF was added before use to make Wash Working Buffer.

Elution Buffer

200mM Glycine pH: 2.5

The prepared buffer was stored at -80°C.

Neutralization Buffer

1M Tris pH: 6.8

The prepared buffer was stored at -80°C.

3.2 Methods

3.2.1 Experimental design

This thesis is about finding novel interaction partners of ATG3 when autophagy and mitophagy are induced. Firstly, cells were transfected with different transfection reagents. ATG3 was over-expressed in Hep3B cells and then induced with autophagy and mitophagy modulators. ATG3 was pulled down by agarose beads and samples were analyzed with LC-MS/MS and bioinformatics tools (Figure 5).

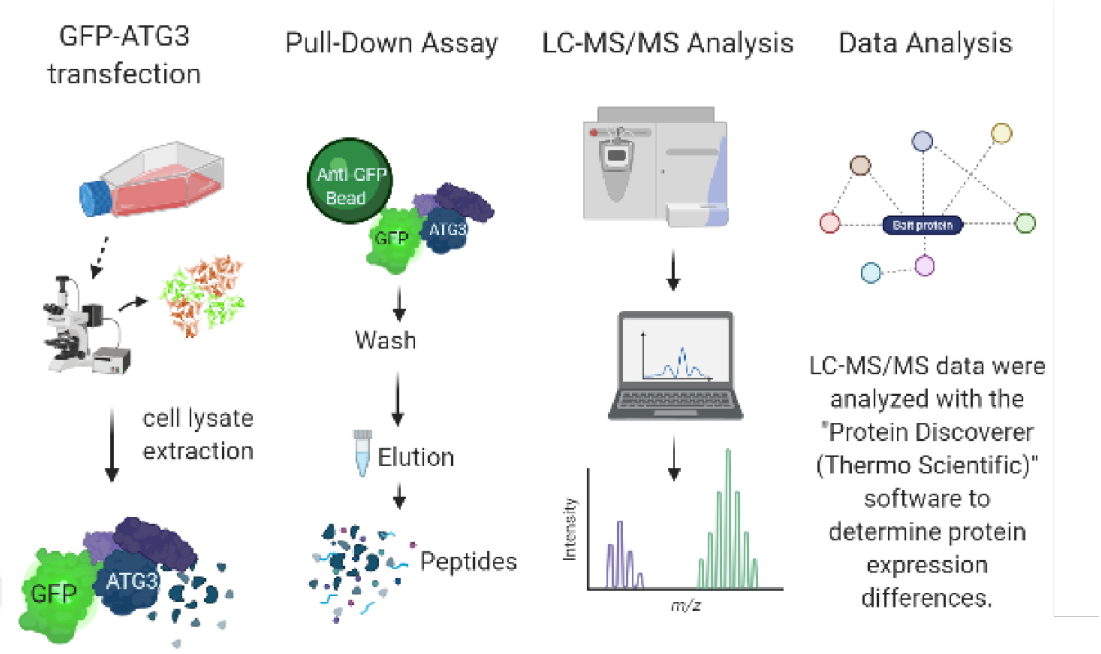

Figure 5. Experimental design

3.2.2 Cell culture

Hep 3B2.1-7 hepatocellular carcinoma cells were obtained from ATCC. The cells were cultured in DMEM high glucose medium supplemented with 1% penicillin-streptomycin and 10% sterile fetal bovine serum (FBS) in a humidified atmosphere of 5% CO_2 at 37°C. The cells were passaged twice a week and subcultured as the manufacturer's recommendation.

3.2.3 Protein isolation

Hep3B cells were seeded at $12x10^4$ density in 12 well-plate. Cells were incubated in a 5% CO_2 incubator for at least 24 hours until cells were attached. Cells were incubated with increasing concentrations of CCCP (1 µM, 5 µM, and 10 µM) and Torin 1 (50 nM, 100 nM, and 200 nM) with varying incubation times (1 h, 2 h, and 4 h). After treatment of cells with CCCP and Torin, cells were removed by PBS and cell pellets were collected. The cell pellets were dissolved with 1X RIPA buffer containing 1X protease inhibitors for 10 minutes on ice by pipetting. After 10 minutes, suspensions were pipetted once more and incubated for another 10 minutes on ice.

Afterwards, suspensions were centrifuged at 14000 g for 10 mins at 4°C. The supernatants were stored at -20°C.

3.2.4 Protein concentration determination

Protein concentrations were determined by Bradford Assay using BSA as a standard. For this purpose, 1 µg/µl BSA was prepared and diluted by serial dilution to lower concentrations (0.5, 0.25, 0.125, and 0,0625) to create a standard curve. Each protein was diluted in ddH_2O at a 1:10 ratio and put into a 96-well plate in triplicates. As a blank ddH_2O was used. 5X Bradford reagent was diluted to 1X Bradford reagent as the manufacturer's recommendation. 10 µl of each diluted protein sample were mixed with 190 µl 1X Bradford reagent and incubated at room temperature for 10 minutes. After 10 minutes of incubation, the plate was read at 596 nm. Mean values of each sample and BSA standards are calculated. Protein concentrations of unknowns are calculated according to the equation obtained from BSA standard curves.

3.2.5 Western blotting

10 µl total protein was mixed with diluted from 5X Loading Buffer to 1X and boiled at 95°C for 5 minutes. Boiled samples were placed on ice and centrifuged at maximum speed for 1 minute. Protein samples were loaded onto 12% and 15% SDS-PAGE gels to detect high and low molecular weight proteins, respectively. Samples were run at 80V for an hour then 100V until samples reach the bottom of the gel. 12% gels were transferred onto nitrocellulose membrane for 45 minutes and 15% gels were transferred onto 0.22 µm PVDF membrane for 30 minutes using the Bio-Rad semi-dry blotting system. After blotting membranes were blocked by 5% skimmed milk for 1 hour at room temperature. Blotted membranes were incubated with primer antibody overnight at 4°C. Primary antibody dilution can differ according to the type of antibody. Diluted primary antibody conditions were used as rabbit anti-LC3B 1:5000, mouse anti-β-Actin 1:10000, mouse anti-p62 1:2000, and rabbit anti- PINK-1 1:2000. Membranes were washed with 1X PBS-T for 10 minutes three times to apply a secondary antibody. Peroxidase conjugated secondary antibody 1:10000 mouse and 1:10000 rabbit were applied to membranes for 1 hour at room temperature. Membranes

were washed with 1X PBST two times and lastly washed with 1X PBS for 10 minutes. Protein bands were visualized with SuperSignal West Pico chemiluminescent solution in ChemiDoc (Bio-Rad). Protein bands were analyzed with ImageLab software.

3.2.6 Competent cell preparation and plasmid isolation

5 µl of competent cell DH5α was mixed with 5 ml LB (liquid broth) and the cells were incubated at 37ºC overnight in a shaker. 500 µl of growth culture was mixed with 10 ml Zymo Broth Media and incubated at 30ºC at 200 rpm. The culture OD was followed by the spectrometer at 600 nm until colonies reached between 0.6-0.8 OD. At this point, the growth culture was collected and incubated on ice for ten minutes. Then the culture was centrifuged at 2200 g for ten minutes at 4ºC. The supernatant was discarded, and the pellet was dissolved with wash buffer. The tube was centrifuged at 2200 g for ten minutes at 4ºC. Pellet was dissolved with 1ml competent buffer and aliquoted for storage at -80º C.

mEmerald-ATG3-N-18 (#53999) and mEmerald-N1 (#53976) plasmids were purchased from Addgene and produced using DH5α cells. A single colony was chosen for plasmid isolation assay and added into a 5 ml medium followed by incubation overnight at 37ºC on a 220 rpm shaker. ZymoPURE miniprep Plasmid kit was used for the isolation of plasmids. After isolation, plasmids' concentrations were measured by NanoDrop and stored at -80ºC (Table *9*).

Table 9. Plasmid DNA Concentration

Plasmids	**A 260**	**A280**	**A260/ A280**	**A260/ A230**	**Concentration (ng/ µl)**
mEmerald-ATG3-N-18	4,32	2,24	1,93	2,27	216,2
mEmerald-N1	7,57	4,00	1,89	2,23	193,3

3.2.7 Plasmid transfection with Lipofectamine 3000

Hep3B cells were seeded at $3x10^6$ density in 10 cm petri dishes. Dishes were incubated overnight at 5% CO_2 at 37°C incubator for cell attachment. When cells reached 70% fluency transfection started. 500 µl OPTI-MEM medium were added to two different centrifuge tubes. Plasmid DNA 12 µg and 28 µl P3000 buffer (Lipofectamine 3000) were added into the first tube and pipetted gently. Lipofectamine 3000 Reagent 22 µl was added to the other tube and pipetted gently. Two centrifuge tubes were mixed and allowed to mix well by pipetting. The mixed solution was incubated for 15 minutes at room temperature. After that solution was added by droplets onto cells which were seeded at 10 cm dishes. Cells were controlled within 48 hours following transfection and observed with fluorescent microscopy.

3.2.8 Plasmid transfection with Pei-max

Hep3B cells were seeded at $20x10^5$ for each well in a 12-well plate. Cells were incubated overnight at 5% CO_2 at 37°C incubator for cell attachment. 100 µl OPTI-MEM was separated into two microcentrifuge tubes. 1 µg Pei-Max was added to the first tube. 1 µg plasmid DNA was added to the second tube. Tubes were mixed gently and incubated for 30 minutes at room temperature. A mixed solution was applied as a droplet onto cells. Cells were controlled following 48 hours of fluorescent microscopy.

3.2.9 Determination of the cytotoxic effect of transfection agents

Hep3B cells were seeded in a 96-well plate at $10x10^3$ density. Cells were incubated overnight at 5% CO_2 at 37°C incubator for cell attachment. Cells were transfected with Lipofectamine 3000 and Pei-Max. Cells were observed for 48 hours and a 10 µl MTT reagent was added to cells and incubated for 4 hours in an incubator. 100 µl Solubilization buffer was added into each well of the microplate. The plate was incubated overnight at 5% CO_2 in a 37°C incubator. Purple formazan crystals were visualized in a 96-well plate. The plate was measured by microplate reader VarioSkan. Spectrophotometrical absorbance values were measured between 590 and 600 nm. Data from measurement were analyzed and used to draw a bar graph.

3.2.10 Pull down of ATG3

Hep3B cells were seeded at 10 cm petri dishes and transfected with mEmerald-ATG3-N-18 and mEmerald-N1(GFP) plasmids. Transfected cells were induced with Torin 1 and CCCP modulators separately. Cells were trypsinized and collected into microcentrifuge tubes. Cell pellets were dissolved with extraction buffer and homogenized with KONTES® DUALL-20 glass tissue grinders. Homogenized cells were centrifuged at 18000 g for ten minutes at 4°C. In this process, a small number of samples were collected as low-speed supernatant (LSS). Supernatants were displaced into TLA-110 ultracentrifuge tubes and centrifuged at 100000 g for an hour to obtain cell lysate (high-speed supernatant, HSS). 50 µl of GFP-Trap® agarose beads were added inside of Zeba™ Spin Desalting Columns. Columns were placed into new centrifuge tubes and centrifuged at 2500 g for 3 minutes. Beads were washed with 250 µl of wash buffer and centrifuged at 2500 g for 2 minutes twice. 100 µl of lysis buffer was added into beads to get through from the column lastly. After ultracentrifugation supernatants were added to Zeba columns. Columns were incubated on a shaker at 4°C for an hour. Columns were placed into new centrifuge tubes and centrifuged at 2500 g for 2 minutes and flow is collected as unbound samples. Columns were placed into new microcentrifuge tubes and 300 µl wash buffer was added into the sample then this process was repeated 3 times to ensure washing properly. 10 µl of Neutralization Buffer was added into new microcentrifuge tubes and columns were placed onto tubes after washing steps and 100 µl elution buffer was added into the beads. Tubes were incubated for 5 minutes on ice and centrifuged at 2500 g for five minutes. Eluted samples were frozen with liquid nitrogen and stored at -80°C.

3.2.11 Sample purification

Samples were purified before dyeing with Cy3 and Cy5 DIGE. 100 µl of eluted samples were mixed with 400 µl methanol. Samples were vortexed gently and centrifuged at 3000 g for 10 seconds. 100 µl of chloroform was added and vortexed gently for five seconds. As the last step, 300 µl sterile water was added. Tubes were vortexed for 5 seconds and centrifuged at 3000 g for ten minutes 4°C. After centrifuge three different phases have formed. The upper phase was removed and 300 µl of

methanol was added for precipitation. Tubes were vortexed for 3-4 seconds. Samples were got cloudy form. Samples were centrifuged at 8000 g at room temperature for 10 minutes. The supernatant was removed and tubes were allowed to air dry for ten minutes on ice. Precipitated proteins were dissolved with 20 µl UTCT buffer and stored at -80°C.

3.2.12 2D gel electrophoresis

Purified samples were dyed with 400 pmol Cy3-NHS or Cy for 30 minutes at room temperature. Unbound dye particles were inactivated with 50 µM L-lysine for the first dimension, samples were dyed with different colors and were mixed and applied to the 7 cm non-linear strips for isoelectronic focusing. Passive rehydration was done overnight. The following day, isoelectronic focusing was run at 150V for 30 mins (rapid), 300V for 30 mins (rapid) and 1000V for 30 mins (linear), 3000V for 2 hours(linear), 3000V for 2 hours (rapid) and hold on 250V. Strips were placed into 14% polyacrylamide gels and filled and fixed with 1% agarose TAE buffer. The gel was run at 200V. The fluorescent dyed gel was scanned on Typhoon 9500. Results were merged and analyzed on the ImageJ software.

3.2.13 Flow cytometry

Hep3B cells were seeded at $20x10^5$ confluency in 12 well-plate. The following day cells were transfected with mEmerald ATG3 N18 and mEmerald N23 plasmids by using Lipofectamine 3000. Cells were visualized for 48 hours for efficient transfection. After that, cells were trypsinized for gentle dissociation from the vessel. Cells were washed with PBS to ensure removing excess medium. Cells were counted with a hemocytometer and calculated at one time $30x10^5$ cells in a flow cytometer tube. Cells were followed by flow cytometer. Non-transfected cell populations were used to define the gate. FITC channel was used to determine percentages of transfected cells.

3.2.14 Protein digestion method

Before LC-MS/MS spectrometer analysis, purified protein concentrations were determined by Qubit Assay and all samples were diluted up to 100 µL and fixed at 50 µg (0,5 µg/µL) with ammonium bicarbonate solution provided in the kit. Protein

samples were transferred in 30 kDa cut-off columns and 200 µl urea was added to each one. Columns were centrifuged at 14000 g for 15 minutes. This step was repeated twice. 100 µl 1x IAA solution was added and vortexed for a minute. After 20 minutes of incubation at dark, samples were centrifuged at 14000 g for 10 minutes. 100 µl urea was added into columns and centrifuged at 14000 g for 15 minutes and the step was repeated twice. 100 µL 50 mM ammonium bicarbonate was added to samples and centrifuged at 14000 g for 10 minutes. This step was repeated two times. 50 µl of digestion solution (20 µg trypsin (Promega) was added (enzyme to protein ratio 25:1). Samples were incubated overnight at 37°C. Columns were transferred in clean tubes. 40 µl 50 mM ammonium bicarbonate was added into columns and centrifuged at 14000 g for 10 minutes. This step was repeated twice. 50 µl 0,5 M NaCl solution was added to samples and centrifuged at 14000 g for 10 minutes. Flow-through peptides were transferred Protein-LoBind tubes and peptides concentrations were determined by NanoDrop. The final value of samples was diluted at 200 ng/µL by using 0,1% Formic Acid solution and stored in convenient tubes for LC-MS/MS.

3.2.15 Chromatography and MS analysis

Thermo Scientific ™ UltiMate ™ 3000 RSLC Ultra Nano high-performance liquid chromatography and Thermo Scientific ™ EasySpray ™, Thermo Scientific Q Exactive ™ HF mass spectrometry was used for the analysis of samples. Calibration has been done before analysis and 2 µg Pierce HeLa Protein Digest Standard (88329) was used for quality control. Tryptic peptides were loaded onto HPLC columns. Peptides were held in columns at first (C18 PepMap100, 5 µm, 100A, 300 µm i.d x 5 mm) and separated with the help of an acetonitrile gradient. After peptides were separated at 300 nL/min speed at HPLC with (Easy-Spray ES804A RSLC C18, 2 µm, 100 A 75 µm x 15 cm) column at 40°C for 50 minutes. 1000 ng peptide was loaded into a 150 mM Nano LC column. Mobile phase A and mobile phase B were set at 0.1%FA, 98:2% H2O: ACN, and 0.1%FA 98:2% ACN: H20 respectively. Q Exactive HF-X device (Thermo Fisher Scientific, Bremen, Germany) was cleaned on the same day and calibrated with Tube (Version 2.9) software. Spray voltage was set at 2kV, funnel RF level 50, and the capillary temperature was set at 270°C. The device had been set on a “Full MS/DD−MS/MS” configuration for data-dependent acquisition.

Full MS resolution was set up m/z 200 for 120000. Full MS AGC target was set IT 100 ms 3E6. The mass interval was defined as 350-1400. MS/MS AGC target value was 5E4 "intensity threshold" 4E4 and isolation spectrum 1,2 m/z. Normalization collision curve energy was 28% and all data were obtained in positive ion mode. Mass analysis and verification were done with TraceFinder ™ software. Discoverer 2.4 software was used for data analysis through the Sequest HT searching algorithm. The files were searched against the NCBI *homo sapiens* (Taxonomy#ID:9606) using the Sequest HT search engine. Request HT parameters were set up primer mass tolerance 10ppm and fragment mass tolerance 0,02 kDa.

3.2.16 Relative group analysis

Discoverer 2.4 software was used to obtain protein expression variation analysis. Each protein sample was analyzed three times and two defined peptides out of three were used. In this way, technical errors and variations were eliminated. Different samples were compared and a diversity of peptides was detected. Different peptides relative to different sample group was defined and listed.

4. RESULTS

4.1 Autophagy and Mitophagy Induction of Hep3B Cells

4.1.1 Autophagy induction of Hep3B cells

In this study, autophagy was induced by using Rapamycin and Torin 1 (inhibitors of the target of rapamycin, mTOR) which are autophagy modulators in hepatocellular carcinoma Hep3B cells. Hep3B cells were seeded into a 12-well plate for Rapamycin treatment in a dose and time-dependent manner. Cells were treated with 50 to 400 nM Rapamycin for 2 and 4 hours to induce autophagy. We observed that the LC3B-II protein level increased within 2 hours upon Rapamycin treatment at doses from 50 nM to 400 nM (Figure 6).

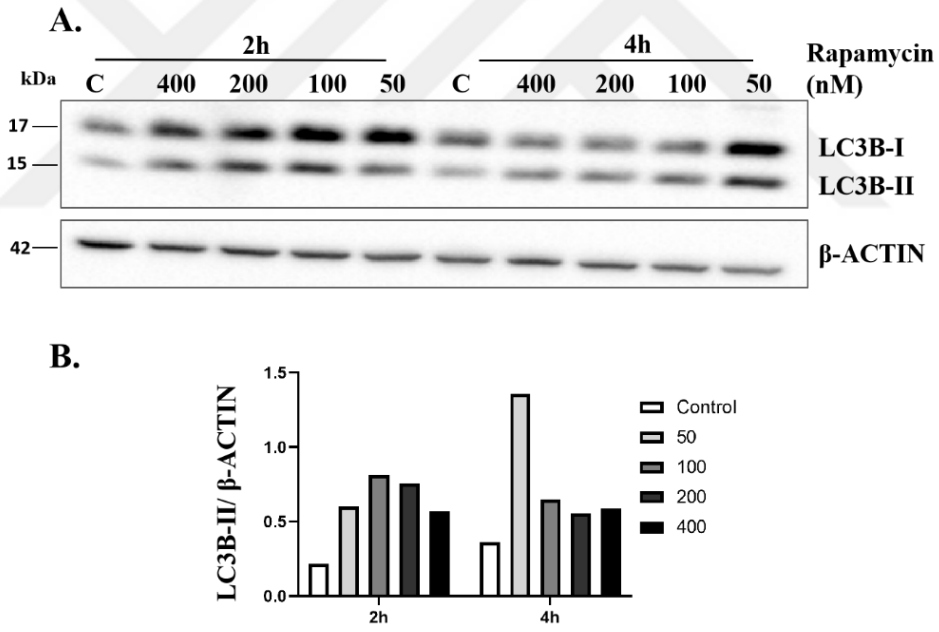

Figure 6. Effects of Rapamycin in the dose and time-dependent manner on Hep3B cells.

((A) Hep3B cells were treated with Rapamycin with (50,100,200 and 400) nM for (2 and 4) hours. β-ACTIN is used as a loading control. Protein band densities were measured by ImageLab software. (B) Measured protein levels were used to perform a bar graph that represents two independent experiments. The bar graph was drawn by GraphPad Prism 8. (*n=2, p-value > 0.05*)

Similar to rapamycin treatment, we treated cells with different concentrations of Torin 1 at different time points (Figure 7A). LC3B-II protein levels increased within the first hour at 50 nM 200 nM Torin 1 treatment. p62 expression levels were also determined to monitor lysosomal degradation. We did not observe statistically significant differences in p62 levels upon 2 hours of induction with 200 nM Torin 1. According to LC3B-II levels, 2 hours of treatment with 200 nM Torin 1 showed the highest autophagy induction.

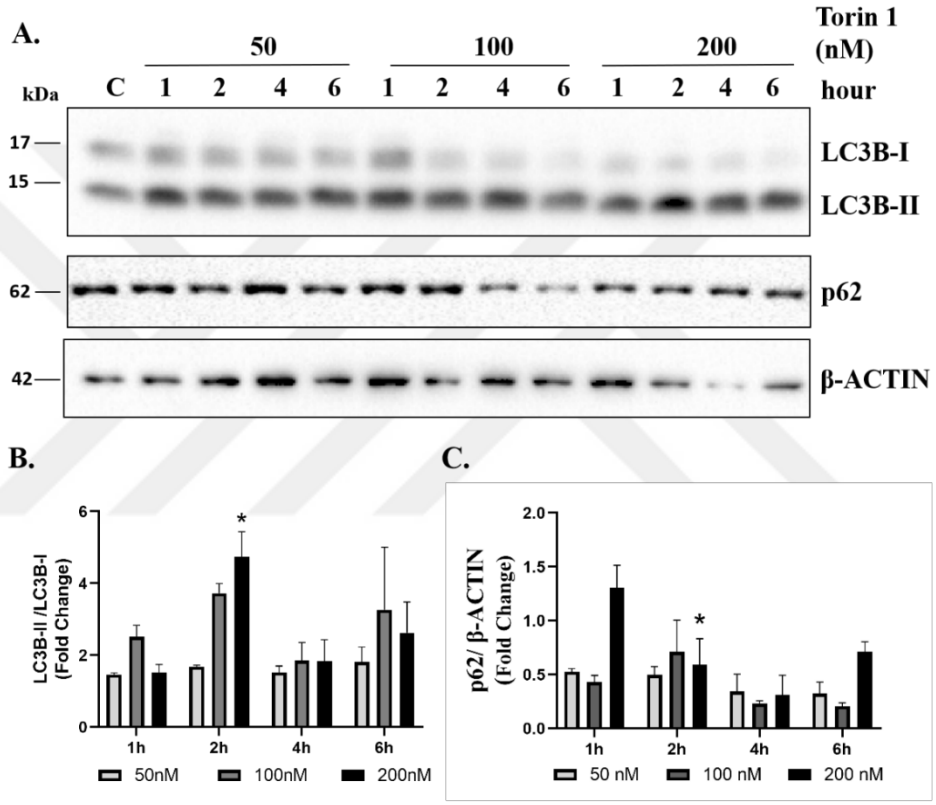

Figure 7. Effects of Torin 1 in the dose and time-dependent manner on Hep3B cells.

((A) Hep3B cells were treated with 50, 100, and 200 nM Torin 1 at 1, 2, 4, and 6 hours. LC3B-I, LC3B-II, and p62 expression levels were represented. β-Actin is used as an internal control. Protein bands were analyzed with ImageLab software. (B and C) Data were normalized compared to control and bar graphs were drawn by GraphPad Prism 8 software based on six independent experiments. (n=6, *p-value 0.025 for LC3B-II/LC3B-I; n=4 p-value 0.83 for p62/β-Actin)

4.1.2 Mitophagy induction of Hep3B cells

Mitophagy is a selective type of autophagy that is involved in removing and recycling damaged mitochondria. Carbonyl cyanide m-chlorophenyl hydrazine

(CCCP) a molecule known as an uncoupler disrupts mitochondrial membrane potential, inhibits ATP production, and increases ROS production, therefore, it is used as a mitophagy inducer (94). We examined LC3B-II/ LC3B-I ratios to assess mitophagy induction (Figure 8). We observed that optimum mitophagy induction was obtained with 10 µM CCCP after 2 hours of induction.

PINK1 is an important protein to monitor mitochondrial damage. Parkin is activated by PINK1 and PINK1 triggers phosphorylation of other proteins on the outer mitochondrial membrane. Mitochondrial depolarization leads to the accumulation of PINK1 on the mitochondrial membrane. Although the PINK1 level was the highest with 10 µM of CCCP treatment at 2 hours, CCCP treatment did not lead to a statistically significant difference in PINK1 protein level in Hep3B cells (Figure 8C). In some circumstances, PINK1 and Parkin may functionally be unrelated to other selective autophagy pathways, because autophagosome formation starts on the surface of mitochondria rather than the isolation membrane (95).

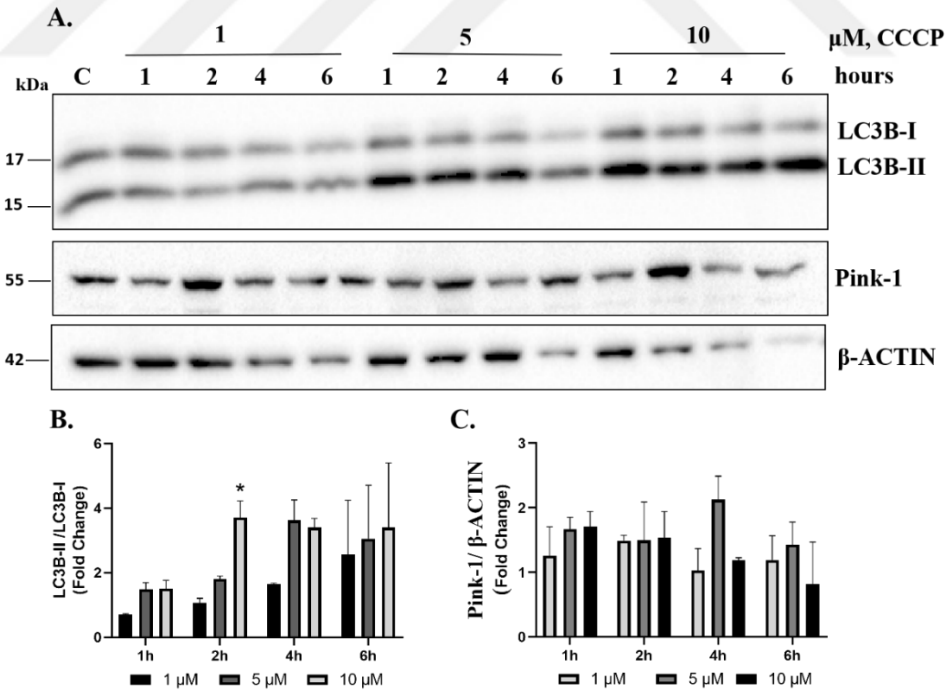

Figure 8. Effects of CCCP in the dose and time-dependent manner on Hep3B cells.

((A) Hep3B cells were incubated in the presence and the absence of CCCP with 1, 5, and 10 µM for 1,2,4, and 6 hours. LC3B-I, LC3B-II, and p62 levels were represented. ß-ACTIN is used as an internal control protein. (B and C) Protein band densities were analyzed by using

ImageLab software. Bar graphs were drawn by GraphPad Prism 8. (n=9, *p-value 0.0036 for LC3B; n=4 p value>0.05 for Pink-1)

4.2 Expression of GFP-tagged ATG3 protein in Hep3B cells

In our study, we used mEmerald-ATG3-N18 and mEmerald N1 plasmids. Hep3B cells were transfected with Lipofectamine 3000 Reagent and PEI-MAX. Transfected cells were monitored for 48 hours under a fluorescence microscope (Figure 9). PEI-MAX and Lipofectamine 3000 transfection reagents were compared in terms of transfection efficiency. PEI is a stable cationic polymer that provides positively charged DNA binding to the anionic cell surface. PEI molecules form a complex with DNA and DNA: PEI complex is endocytosed by the cells and DNA is released into the cytoplasm. Besides, Lipofectamine molecules are cationic liposomes with an affinity to binding negatively charged nucleic acid. Liposomes that contain DNA are positively charged on their surface and can bind to plasma membrane that is negatively charged. Liposome helps to enter nucleic acid cargo molecules into the cytoplasm for replication and expression. We have successfully transfected Hep3B cells with mEmerald-ATG3-N18 and mEmerald-N1 plasmids using PEI-MAX transfection reagent at 1:1 ratio and 1.2 ratios for 48 h (Figure 9).

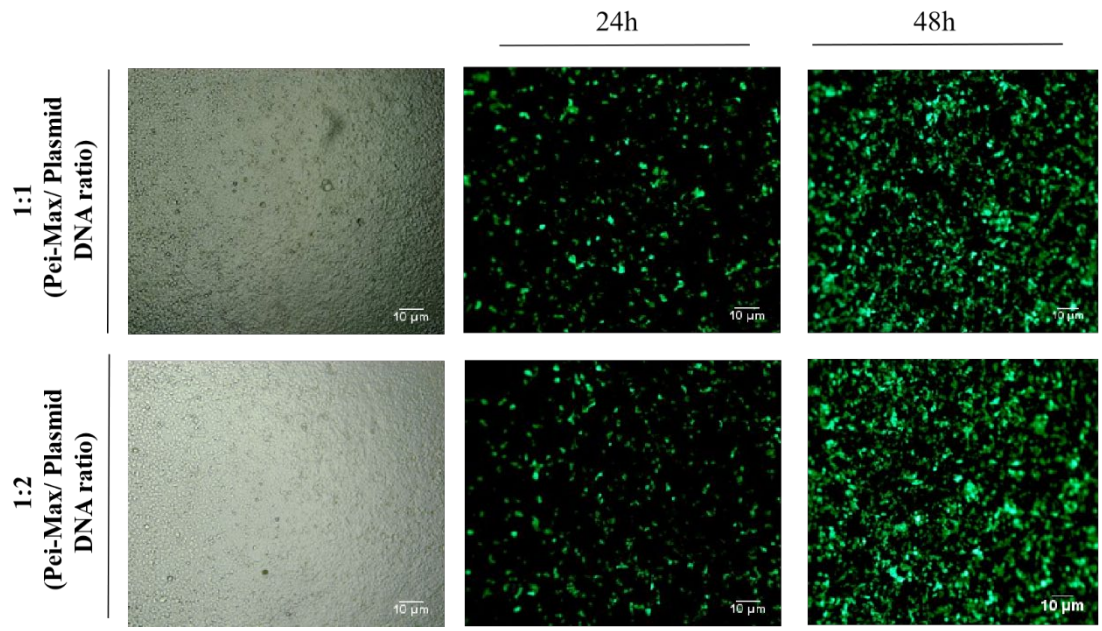

Figure 9. Expression of mEmerald-ATG3 plasmids on Hep3B cells with PEI-MAX.

(Observation of transfected cells on fluorescent microscopy. Cells were transfected at 1:1 and 1:2 ratio (transfection reagent (µg/ µl): plasmid (µg)) and later they were examined on fluorescent microscopy under the FITC channel until 48 hours. Images are taken under 10X magnification. Scale bars were drawn by ImageJ software. (Scale bar, 10 µM.))

Lipofectamine 3000 is a transfection reagent that provides high transfection efficiencies for even hard-to-transfect cells. For this purpose, we tried different ratios of plasmid and reagent concentrations, but the manufacturer's standard protocol yield the best transfection rate. We chose to perform our experiments with 0.15 µl Lipofectamine reagent with a 200 ng plasmid for 48 hours (Figure 10).

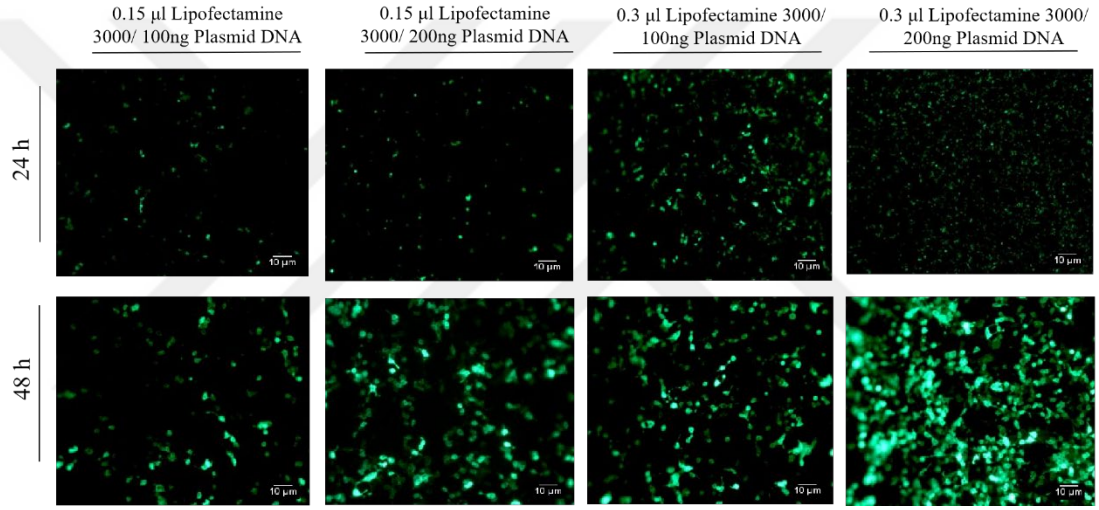

Figure 10. Expression of mEmerald-ATG3 plasmids on Hep3B cells with Lipofectamine 3000.

(Examining of transfected cells with Lipofectamine 3000 on fluorescent microscopy. 0.15 µl and 0.3 µl Lipofectamine 3000 reagent mixed with 100 ng and 200 ng plasmids, separately. Cells were examined for 24 and 48 hours under fluorescent microscopy FITC channel. Images were taken under 10X magnification. The scale bar was drawn by ImageJ software, (Scale bar, 10 µm.)

4.3 Determination of Transfection Efficiency

To quantify transfection efficiency, we also followed transfected cells by flow cytometry. Cells were read in the FITC channel cause mEmerald (modified version of GFP) (Figure 11). Before every pull-down experiment, transfection efficiency was

checked by flow cytometry and if it was lower than 50%, we did not continue our experiment.

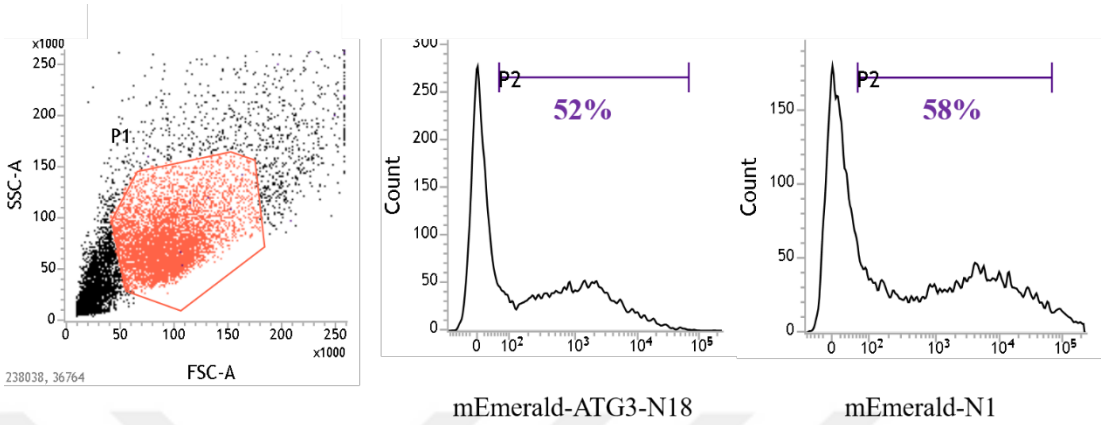

Figure 11. Determination of transfection efficiency with Flow Cytometry.

(Hep3B cells were transfected with mEmerald-ATG3-N18 and mEmerald-N1 plasmids and non-transfected cells were collected by trypsin. Signals from transfected cells were measured on the FITC channel. mEmerald (GFP) vector which is the backbone(empty) vector had 58% and mEmerald-ATG3-N18 had 52% efficiency. The population was chosen from the non-transfected control group. Data represent one example of five independent experiments. Percentages were analyzed with BD FACSuite software.)

4.4 Cytotoxic Effect of Transfection Reagents

Transfection reagents may have cytotoxic effects on cell lines. Transfection reagents themselves, not nucleic acids, often cause this effect. To follow the cytotoxic effect of Lipofectamine 3000 and PEI-MAX, the cell viability of transfected cells was measured by using MTT at 48 hours. MTT reagent was added to cells and after 4 hours of incubation, solubilization buffer was added for overnight incubation. Formazan crystals were checked, and the absorbance was measured at 570 nm. We found that Lipofectamine 3000 showed a less cytotoxic effect than PEI-MAX (Figure 12). However, according to our results, both reagents had a negligible cytotoxic effect on Hep3B cells.

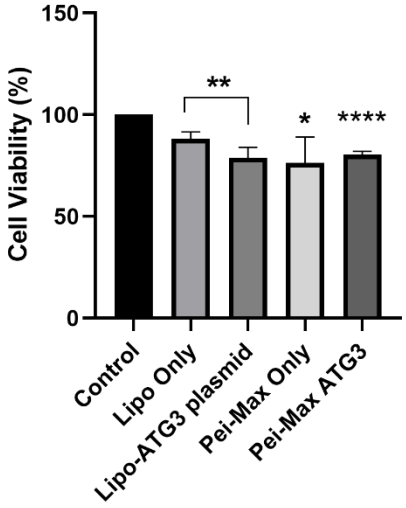

Figure 12. Cytotoxic effects of transfection reagents on Hep3B cells.

(Non-transfected cells were used as control. Only reagents were also used to examine the difference when mixed with plasmids. 0.15 µl Lipofectamine 3000 reagent was mixed with 200 ng. 0.2 µl Pei-Max was mixed with 200 ng plasmids to perform these experiments. The absorbance of the formazan crystals was measured with Varioskan. The bar graph represents the mean ± SEM values of three independent experiments. (*p-value 0.0316, **p-value 0.038, 0.020 ****p value<0,0001))

4.5 mEmerald-ATG3 Plasmid Pull Down

GFP-Trap beads which have a high binding capacity to GFP proteins were used in pull-down experiments. Pull-down assay samples were monitored by SDS-PAGE at all steps including lysis, wash, and elution. Based on our western blot analysis, free GFP protein was present in the lysate (LSS) and input (HSS). However, unbound samples also had free GFP protein bands, indicating the maximal binding capacity of beads was exceeded. But, the washing steps were successful based on the absence of free GFP bands. We observed free GFP bands in elution samples, confirming that the pull-down experiments were performed as planned (Figure 13A). For confirmation of these results, we also repeated the western blots using an anti-ATG3 antibody which confirmed the presence of ATG3-GFP. In addition, endogenous ATG3 protein was present at ~40-42 kDa (Figure 13B).

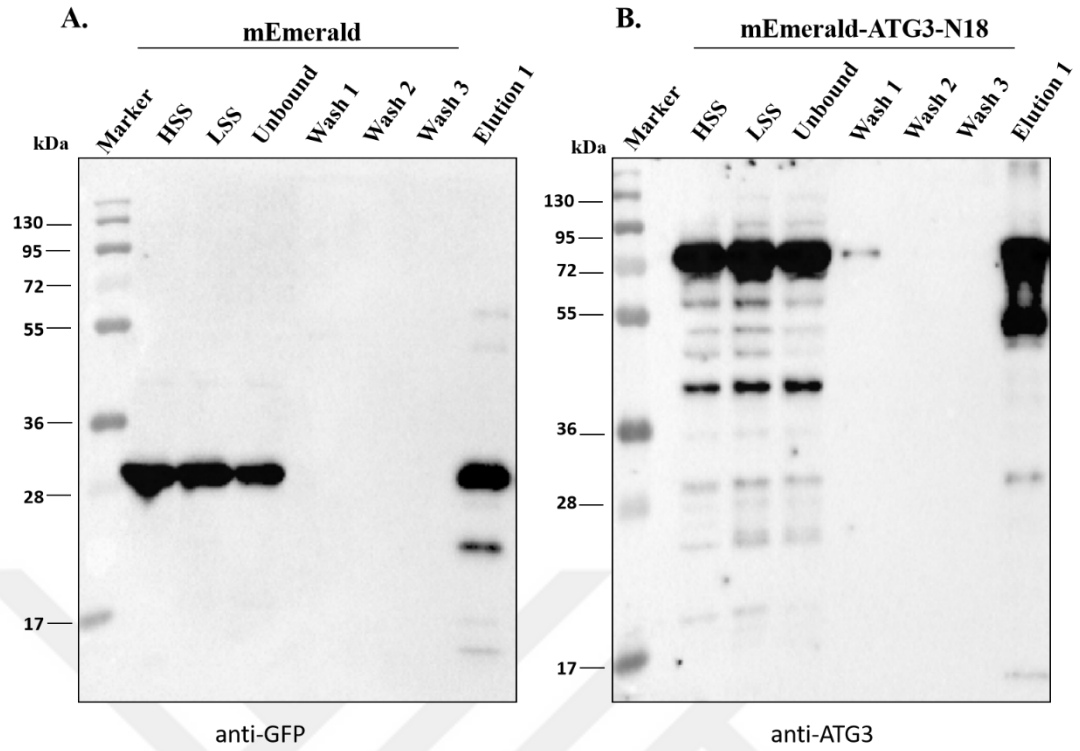

Figure 13. Pull-down assay samples monitoring by SDS-PAGE electrophoresis.

(Samples were collected from the lysis, washing, and elution steps of experiments. (A) Free GFP bands were observed when GFP was eluted. (B) ATG3 protein expression was observed in elution samples. Anti-GFP (1:2000) and anti-ATG3 primary (1:2000) antibodies were used. (HSS: high-speed supernatant, LSS: low-speed supernatant))

Pull-down experiment samples were also analyzed to confirm autophagy and mitophagy induction. According to LC3B-II/LC3B-I protein ratios, both autophagy and mitophagy were successfully induced (Figure 14).

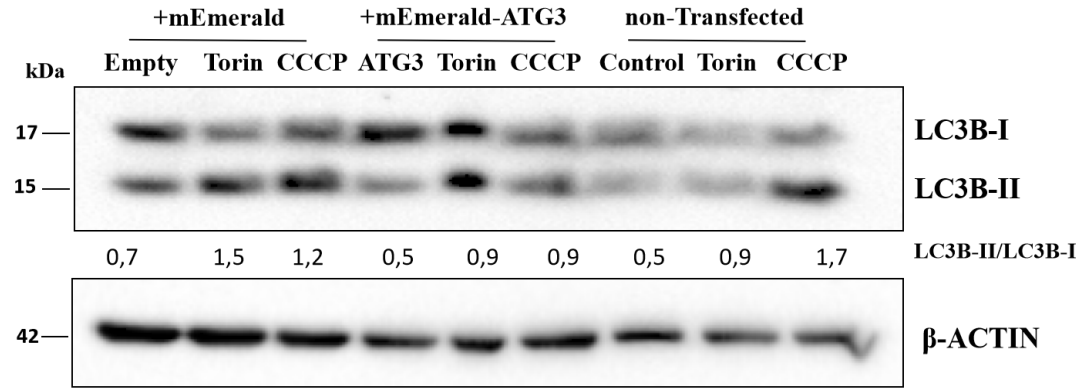

Figure 14. Determination of autophagy and mitophagy induction of pull-down assay samples.

(Autophagy (200 nM Torin 1) and mitophagy (10 μM CCCP) were induced for 2 hours on transfected cells Input samples (HSS) were loaded into 15% gels to perform western blot. Bands were detected with HRP-conjugated chemiluminescent solution. Bands were analyzed with ImgaeLab software. LC3B-II level was normalized by β-ACTIN which is internal control.)

4.6 2D Analysis of ATG3

Pull-down experiments were also analyzed on 2D-PAGEs before mass spectrometry analyses to reveal potential differences between experimental conditions (96). In our initial experiments, we confirmed the pull-downs using 2D-PAGE western blots to monitor ATG3 and GFP (free or conjugated to ATG3, Figure 15). In the next step, pull-down samples were differentially labeled with Cy3 and Cy5 dyes for 2D-DIGE (97) to reveal a qualitative estimate of proteomic differences before LC-MS/MS analysis (Figure 16).

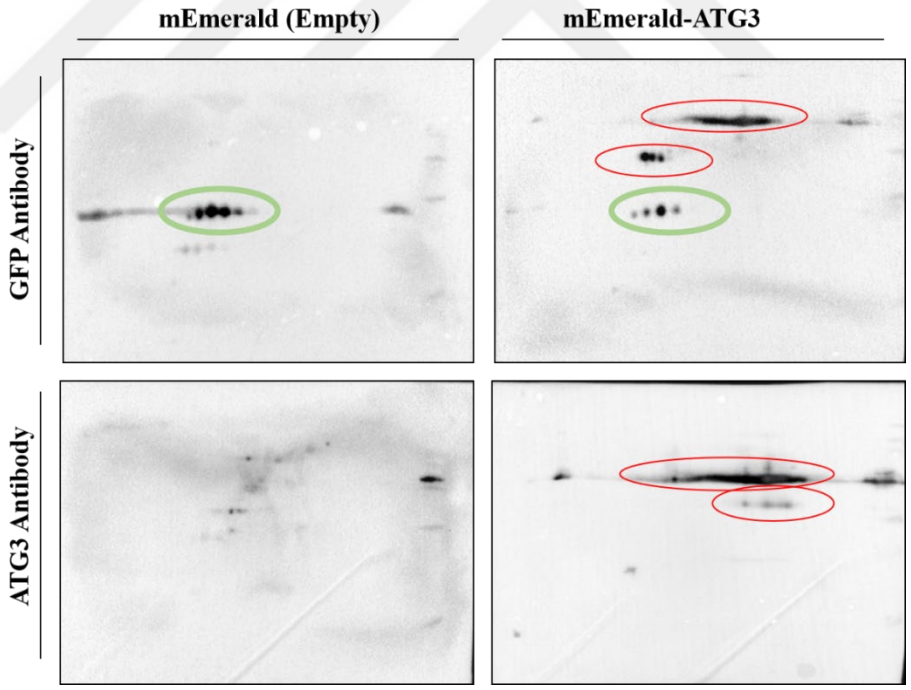

Figure 15. Observation of pull-down samples with 2D gel electrophoresis.

(Following to pull down of ATG3 and backbone vector samples were loaded into 2D gel electrophoresis. After DIGE analysis gels were transferred into the PVDF membrane for antibody treatment. Both antibodies were used to determine the differences between free GFP and ATG3. Membrane images were taken with Bio-Rad Chemidoc by using HRP conjugated solution. Spots encircled in green and red represent free GFP and ATG3 containing protein spots, respectively.)

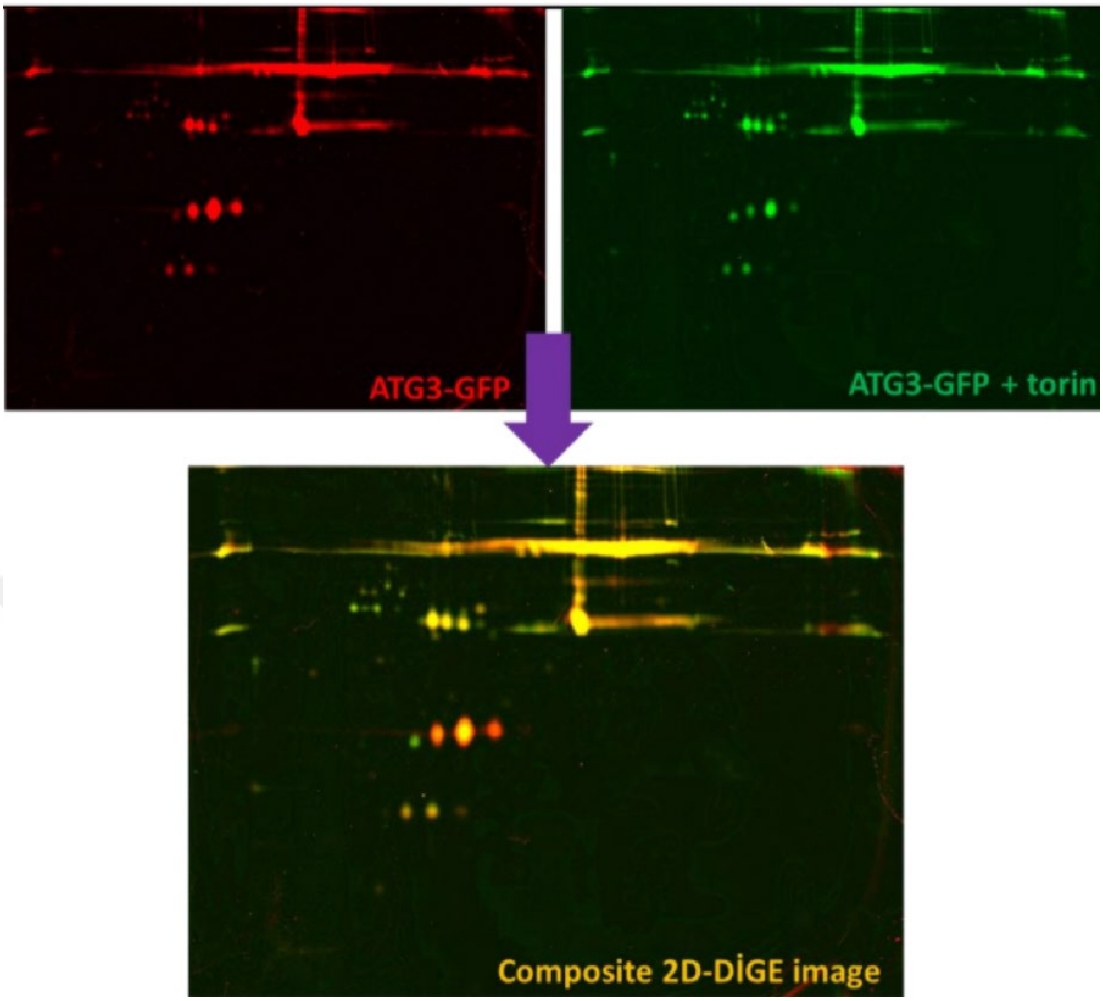

Figure 16. Comparison of pull-down samples with two-dimensional fluorescence difference gel electrophoresis (2D-DIGE).

(Screened proteins are associated with ATG3 overexpression on Hep3B cells. (A) Cells were transfected with ATG3 and labeled with Cy3-NHS ester red as control. (B) Cells were transfected with ATG3 and treated with 200 nM Torin 1 for 2 hours and labeled with Cy5-NHS ester green. (C) The merged image represents Cy3 and Cy5 stained proteins. The gels were analyzed with Typhoon 9500 biomolecular imager.)

4.7 LC-MS/MS Bioinformatic Analysis of ATG3 Partners

The fundamental aim of this study was to find binding partners of ATG3 in the presence of autophagy and mitophagy inducers using LC-MS/MS. Mass spectrometry data of ATG3 pull-downs analyzed with Protein Discoverer (Thermo Scientific) were filtered with the following criteria; 1) protein levels are statistically different from the control group (GFP only) samples ($p<0,05$), 2) protein levels are at least 70% or more compared to the control group, 3) proteins are identified with at least 2 unique peptides.

According to this filter, we identified 98 binding partners for ATG3. Significant protein interactions among these proteins were analyzed with STRING (Figure 17).

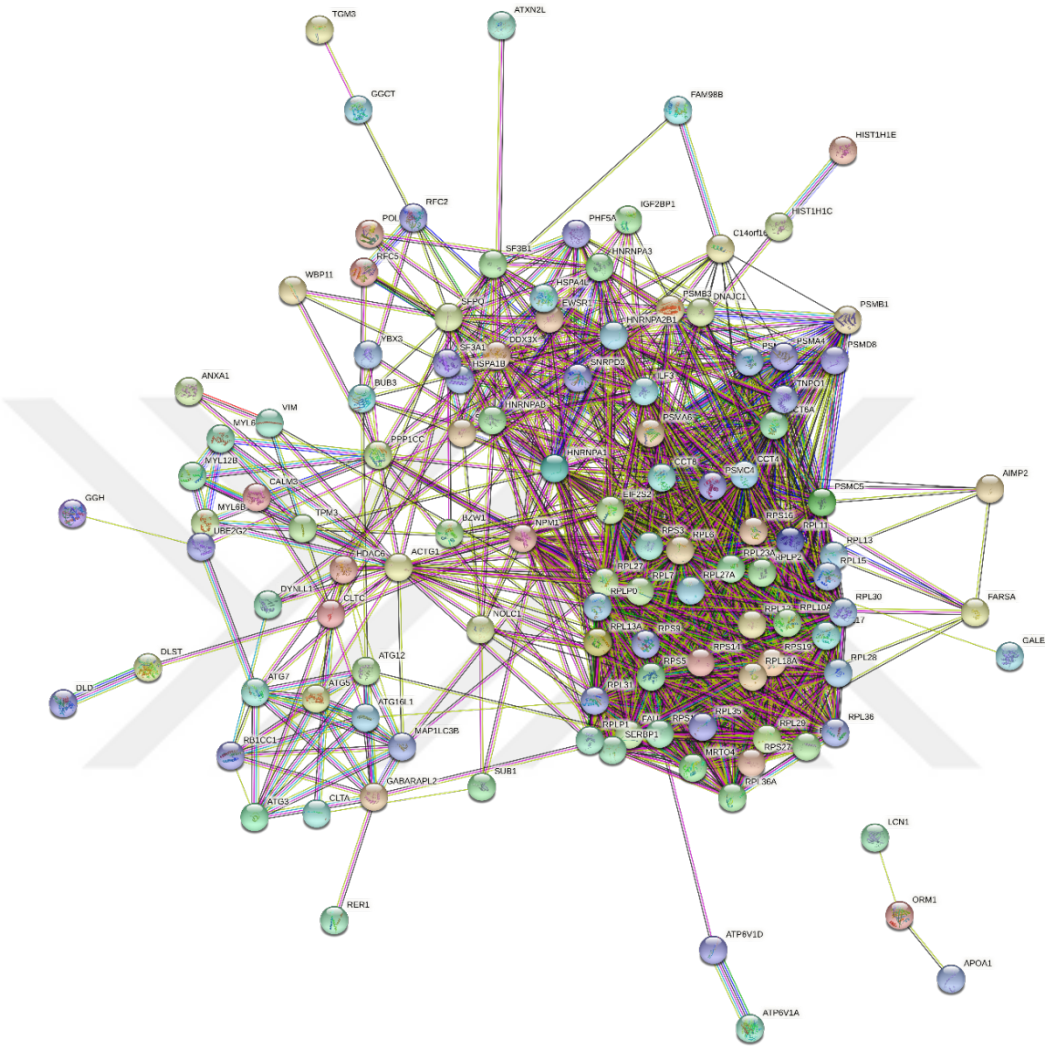

Figure 17. STRING analysis of binding partners of ATG3.

We repeated the STRING analysis with 10 clusters to group the network of proteins, which are likely to have significant interactions with each other (Figure 18). According to the newly clustered STRING analysis, it became evident that a significant number of ribosomal proteins were identified in our pull-down experiments. Based on this observation, the 60S and 40S ribosomal proteins were eliminated from the analysis list and reanalyzed with the STRING algorithm with 7 clusters to focus

on specialized protein networks among the identified ATG3 protein partners (Figure 19).

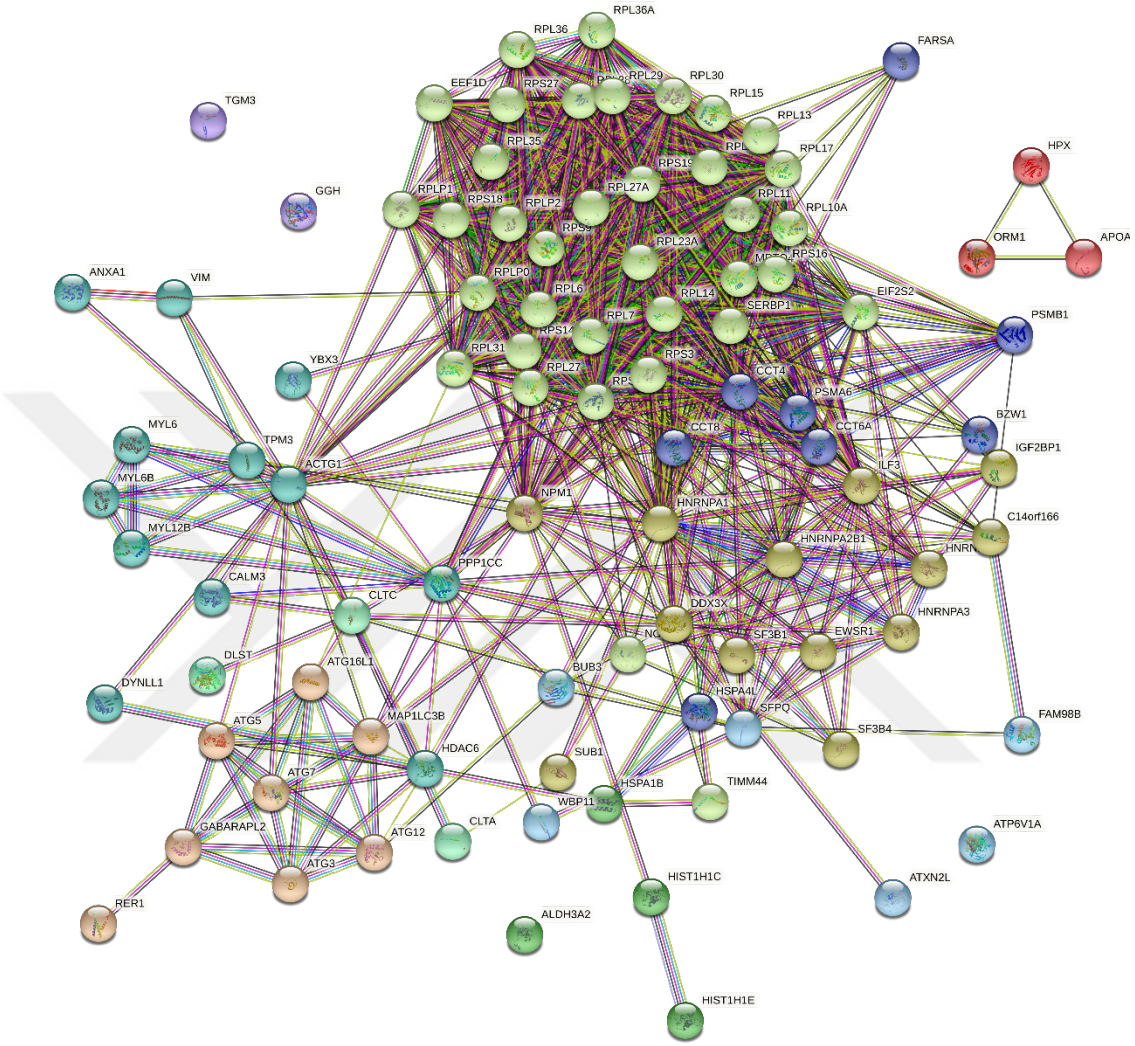

Figure 18. STRING analysis of ATG3's partners based on 10 clusters.

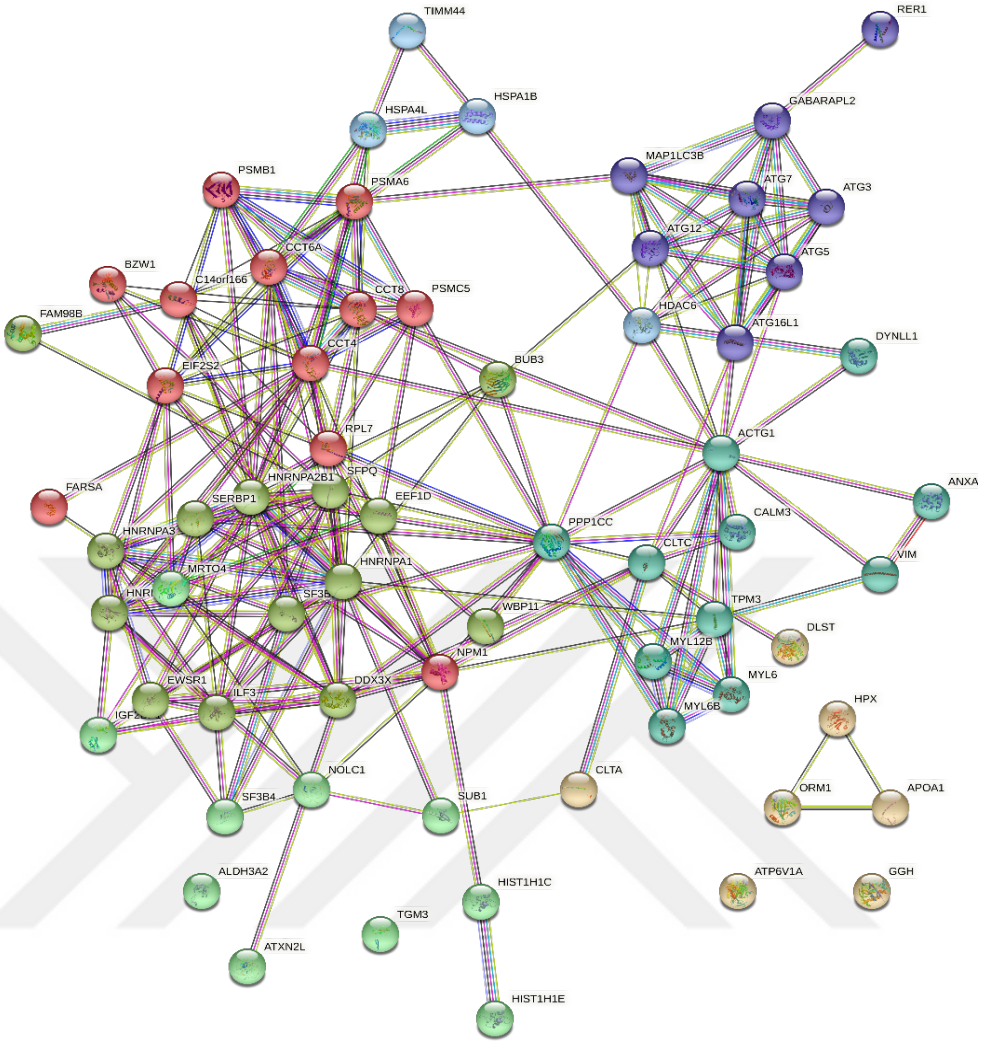

Figure 19. STRING analysis of ATG3's partners based on 7 clusters.

In the same vein and using the same filters, the ATG3-binding proteins during autophagy were identified. After filtering the list for ribosomal proteins, a total of 56 proteins were included in the STRING analysis of autophagy induced groups (Figure 20), and a total of 38 proteins were identified for Mitophagy induced groups (Figure 21).

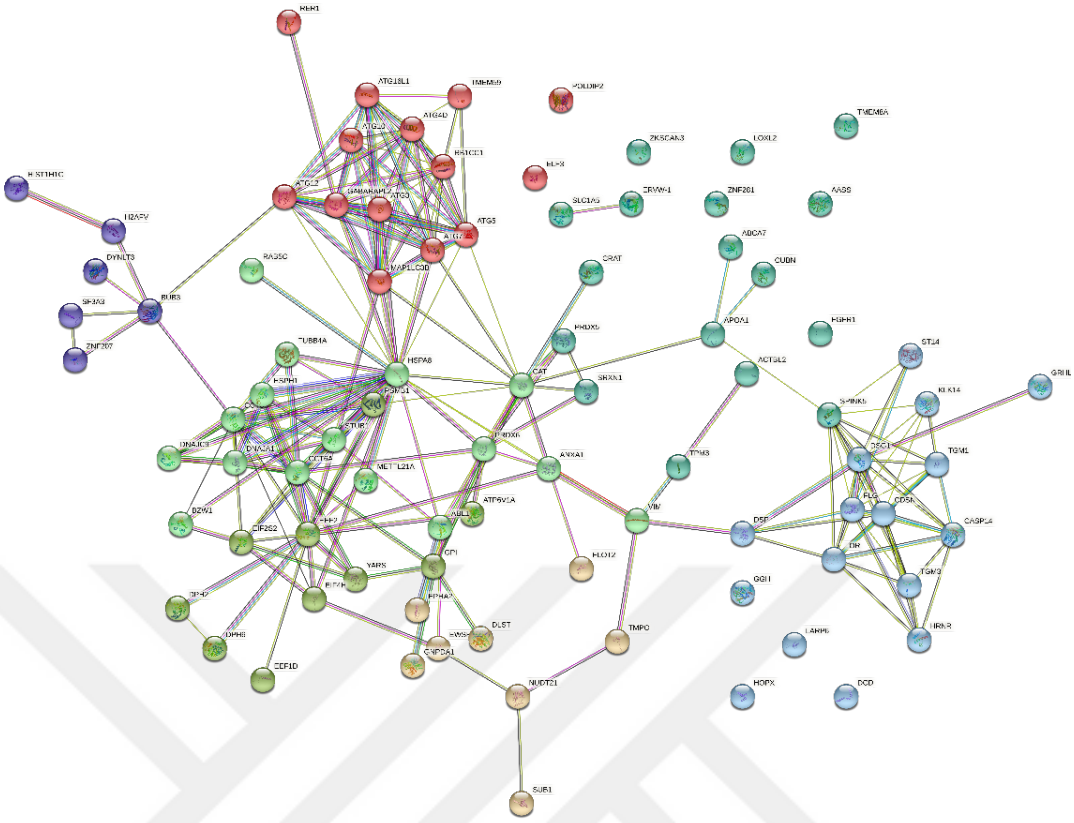

Figure 20. Partners of ATG3 protein in autophagy induced cells.

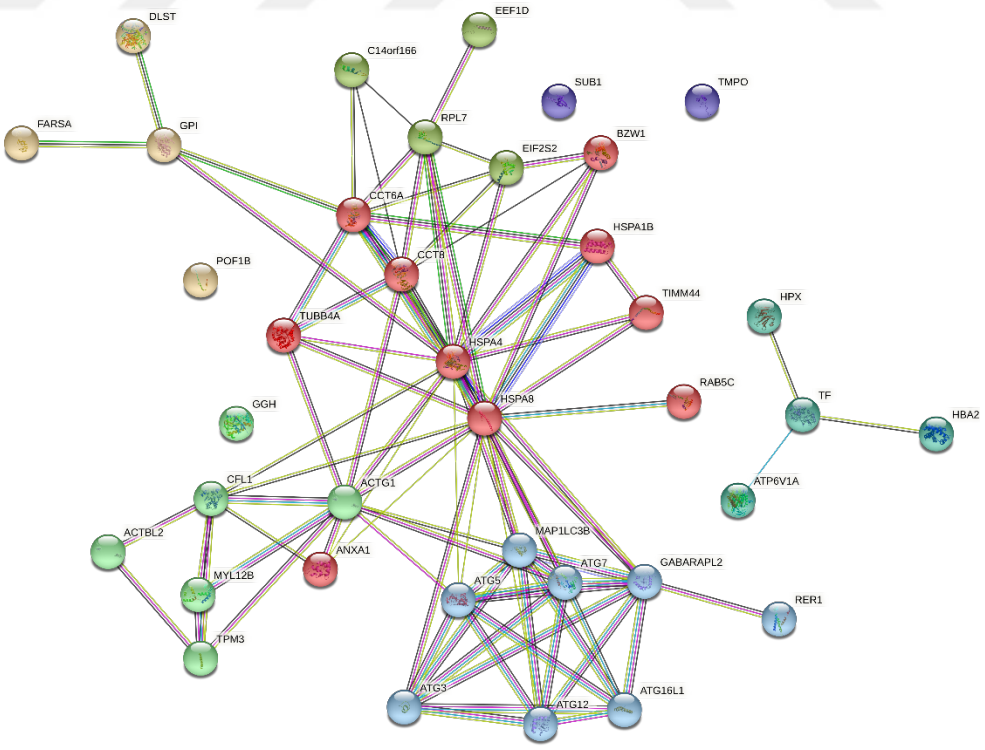

Figure 21. Partners of ATG3 protein in mitophagy induced cells.

When the clusters around ATG3 were compared among control, autophagy induced, and mitophagy induced groups, ATG5, ATG7, ATG12, ATG16L1, MAP1LC3B, and GABARAPL2 proteins were found to be common in three groups (Figure 22).

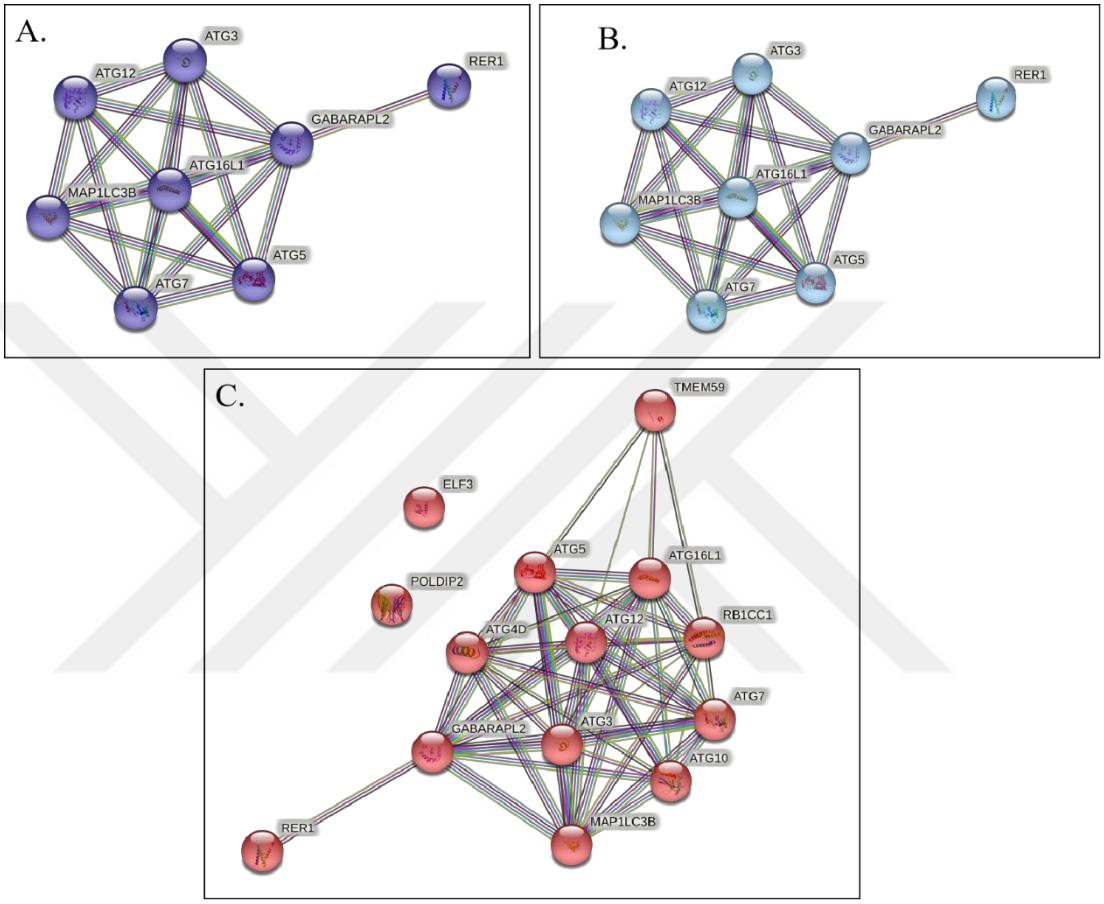

Figure 22. Only ATG3 implicate clusters were drawn from all experimental groups.

((A also purple nodes) represents ATG3. (B also blue nodes) represents Mitophagy induced with CCCP. (C also red nodes) represents autophagy induced with TORIN 1.) Resmin içine yazabilirsin

Next, we identified the common and individual proteins that are found in each experimental group (Table *10*). Based on Venn diagram analysis, 22 of these proteins were common for three groups while 31 proteins were specific to ATG3. Moreover, ATG3 had 8 protein partners specific to mitophagy and 19 protein partners specific to autophagy (Figure 23).

Table 10. List of Common and Individual Proteins

ATG3, Autophagy, and Mitophagy	TPM3, MAP1LC3B, ATG5, ATG7, ATG3, GGH CCT6A, ANXA1, RPL7, C14orf166; RTRAF, ATG12, SUB1, EIF2S2 ATP6V1A, DLST, CCT8, EEF1D, ATG16L1, RER1, HSPA1B; HSPA1A GABARAPL2, BZW1
ATG3 and Mitophagy	MYL12B; MYL12A, TIMM44, HPX, FARSA, ACTG1
ATG3 and Autophagy	PSMB1, BUB3, APOA1, EWSR1, HIST1H1C, TGM3, VIM
Autophagy and Mitophagy	TMPO, ACTBL2, HSPA8, TUBB4A, GPI, RAB5C
ATG3	ATXN2L, ORM1, HNRNPA3, SFPQ, NOLC1, PPP1CC, PSMA6, HNRNPA1 CCT4, MYL6B, HNRNPA2B1, CLTA, CLTC, MYL6, CALM3; CALM2, CALM1, HSPA4L, NPM1, DYNLL1, PSMC5, MRTO4, ALDH3A2, WBP11, HNRNPAB, IGF2BP1, SERBP1, SF3B1, HDAC6, SF3B4, ILF3, HIST1H1E, DDX3X
Mitophagy	RPL27, CFL1, RPL29, HSPA4, HBA2; HBA1, RPLP0, RPL36, POF1B
Autophagy	PRDX6, POLDIP2, FLOT2, TGM1, CDSN, EIF4H, SLC1A5, CASP14, NUDT21, LOR, DSG1, EEF2, YARS, SF3A3, DSP, RPL36A, RPL15, H2AFV, DCD

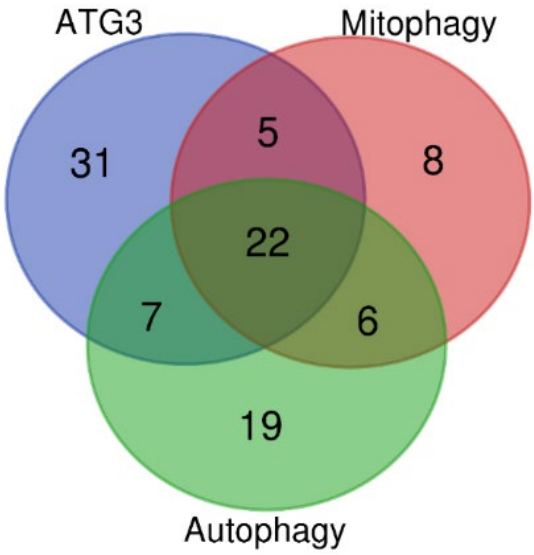

Figure 23. The Venn diagram representing individual and common proteins belonging to experimental groups.

(Bioinformatics & Evolutionary Genomics online Venn diagram tool was used to the representative image of the Venn diagram.)

A Reactome pathway analysis was performed using the false discovery rate (FDR) values calculated from STRING analysis (Figure 24).

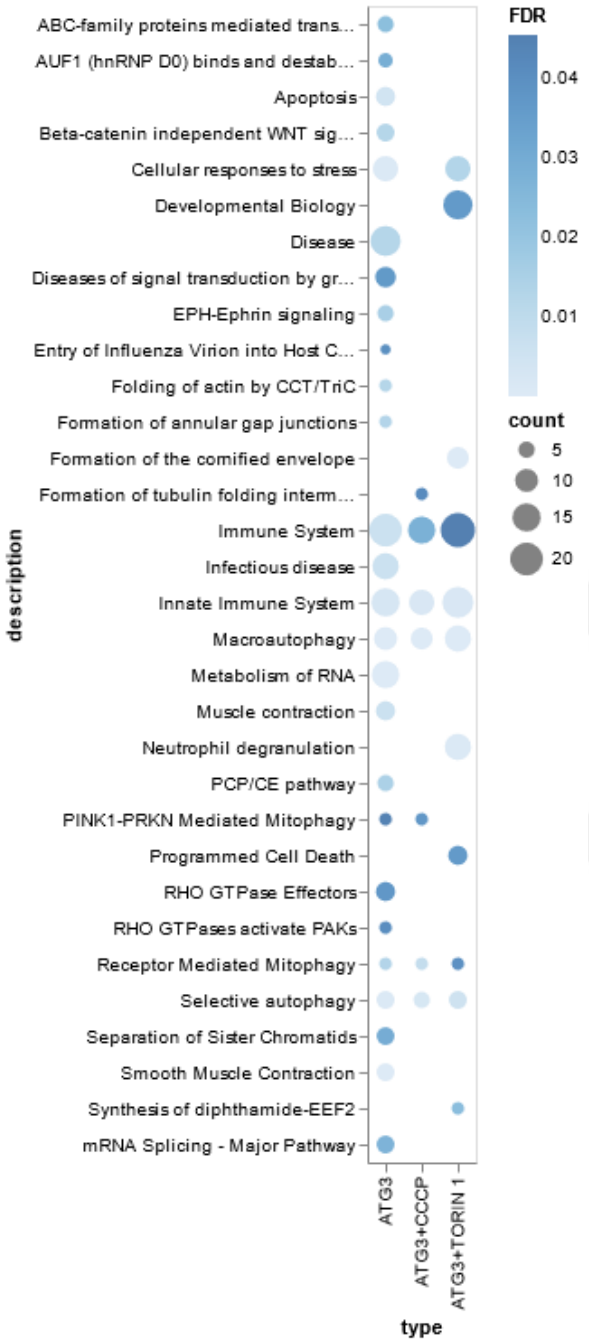

Figure 24. Reactome pathway analysis.

(The most expressed proteins are displayed on the graph following viral gene expression. Pathway results are shown with the number of proteins found in the dataset and computed FDRs for pathway enrichment.)

To validate our pull-down experiments, we performed western blot analysis with elution samples against ATG12 and ATG7. ATG12 was observed in all experimental

groups. Likewise, ATG7 was found to interact with ATG3 in control, mitophagy induced and autophagy induced groups.

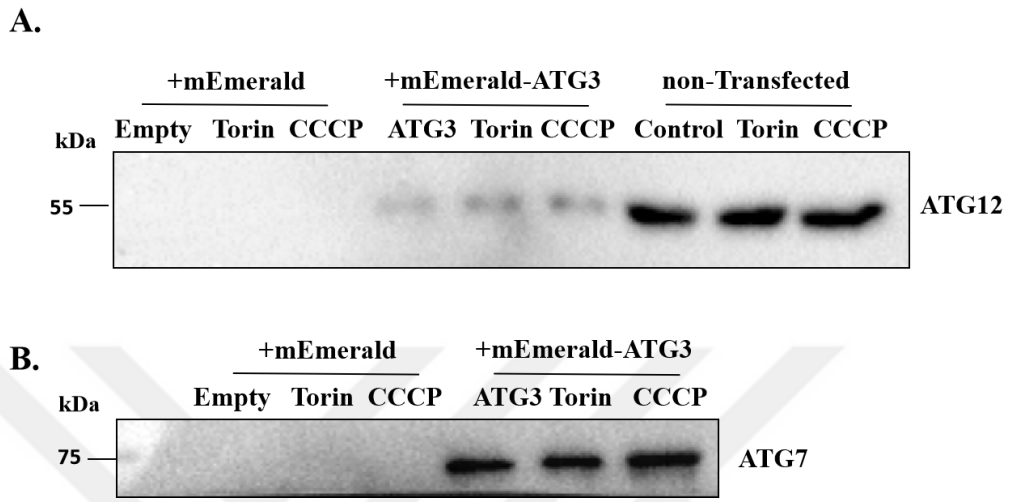

Figure 25. Determination of common ATG3 partner proteins by western blot analysis.

(After ATG3's pull-down common proteins that have interaction with ATG3 were checked. 8 µl of the sample was mixed with 2 µl loading buffer and heated to 95ºC for five minutes. (A) samples were loaded into 15% gel and transferred to PVDF membrane. 1:2000 ATG12 primary antibody was used with 1:5000 Rabbit secondary antibody. (B) Samples were loaded into 12% gel and transferred into a nitrocellulose membrane. ATG7 primary antibody was used with 1:5000 mouse secondary antibody)

5. DISCUSSION

ATG3 is an E-2-like enzyme and has a critical role in autophagosome formation and elongation during the autophagy process. In addition, recent studies have revealed that ATG3 plays a role in mitochondrial quality control, cell death, tumor progression, ischemia-reperfusion injury, degrading pathogens, and cellular homeostasis. The crystal structure of ATG3 showed that it has intrinsically disordered regions which may be involved in dynamic cellular mechanisms (58, 98). Recent studies claimed ATG3 also may have a role in mitosis and cell differentiation in an autophagy-independent manner. Therefore, we investigated the interaction partners of ATG3 during autophagy and mitophagy to find out more about the protein's role in a variety of physiological and pathological circumstances. For this purpose, autophagy and mitophagy were induced in hepatocytes transfected with GFP-tagged ATG3 plasmids. GFP-tagged ATG3 proteins were extracted using affinity purification methods after autophagy and mitophagy induction. To identify ATG3 binding partners, pull-down samples were analyzed using LC-MS/MS mass spectrometry.

Autophagy and mitophagy were induced in Hep3B cells using Rapamycin or Torin 1 and CCCP, respectively. Rapamycin is an autophagy inducer that affects only mTORC1 while Torin 1 is efficient in both mTORC1 and mTORC2. On the other hand, CCCP is an uncoupling agent and increases proton permeability across the mitochondrial inner membranes (99). To monitor autophagy and mitophagy induction, LC3 expression which is the most known autophagy marker was followed by western blot analysis (100). We have successfully induced autophagy by 200 nM Torin 1 treatment (101) and mitophagy by 10 μM CCCP treatment in 2 hours in agreement with the others (102). Protein levels of other autophagy and mitophagy protein markers such as p62 and PINK1 were also monitored. Although we determined decreased levels in both, the results were not statistically significant.

After optimizing the dose and time kinetics, cells were transfected with GFP-tagged ATG3 plasmid and were subjected to immunoprecipitation to pull down ATG3 partners. The GFP-Trap beads (ChromoTek) are made up of an anti-GFP

Nanobody/VHH coupled to agarose beads with a very high affinity (KD=1 pM) to bind even low abundant proteins. This allows the use of GFP-Trap beads for investigating novel interaction partners (103, 104).

Human diseases are frequently caused by dysregulated protein-protein or protein-metabolite interactions (105). Therefore, mass spectrometry-based studies enable unbiased mapping of protein-protein interactions, allowing for the development of novel therapeutic interactions in a variety of diseases (106). Our method was an LC-MS/MS-based approach to find interaction partners of ATG3 similar to the approach used by Mohamed S. Taha and Fereshteh Haghighi in their study to find novel partners of FMRP (107).

The data of ATG3 pull-downs were filtered according to the following criteria: 1) protein levels are statistically different from the control group (GFP only) samples ($p<0,05$), 2) protein levels are at least 70% or more compared to the control group, 3) proteins are identified with at least 2 unique peptides. This analysis led to the identification of 98 binding partners for ATG3. Subsequent analysis with STRING revealed significant interaction networks between the identified proteins.

We observed that 60S and 40S ribosomal proteins were abundant dominant in the interactive maps. Previously, Wang and his colleagues found that mRNA expression was higher in hepatocellular carcinoma tissues than in adjacent nontumor liver tissues. They also indicated that ATG3 overexpression in hepatocellular carcinoma leads to increased autophagic flux (108). Another study claimed that a eukaryotic translation initiation factor (elF5A) is required for LC3 lipidation, and its interaction with ribosomes is enhanced when autophagy is stimulated (109). As a result, we reasoned that the presence of 31 ribosomal proteins was not surprising.

Proteins were defined such as ATG5, ATG12, ATG16L1, ATG7, and LC3 which are known from the literature did not create a fold change between the groups. These proteins are mostly involved in autophagosome formation and during the autophagy

and mitophagy processes. Therefore, it is expected to observe these proteins in all experimental groups.

GABARAPL2 proteins are members of the LC3 protein family, and while they play a role in autophagy, their exact function is unknown (110). In our study, we observed that GABARAPL2 was consistently found in our ATG3 pull-down protein list. Since LC3 collaborates with ATG3 to form autophagosomes, GABARAPL2 may also be involved in autophagosome formation and/or lysosome fusion.

Another intriguing protein is RER1, which is identified in all conditions as an ATG3 binding partner. RER1 participates in the unfolded protein response and is a downstream effector of ER stress (UPR). RER1 contributes to ER homeostasis by transporting misfolded proteins from the ER lumen to the Golgi after autophagosomes have transported them to vacuoles (111).

Another notable protein is RB1CC1, which has never been linked to ATG3. Only autophagy-induced cells showed RB1CC1 protein interaction. According to recent research, the RB1CC1 protein interacts with ATG9A and binds to OPTN to form two distinct axes for autophagic membrane biogenesis on ubiquitin-coated damaged mitochondria (112). The proteins RB1CC1/FIP200, ATG14, and WIPI were upstream factors for autophagosome formation, and they are required for mitochondrial division, whereas ATG3 and ATG5 are not (90). As a result, the RB1CC1 protein may be ATG3's partner protein, especially when autophagy is activated.

According to our data, while 26 proteins were upregulated in the CCCP induced group, 39 of them were upregulated in the Torin 1 induced group. 18 proteins were downregulated when Torin 1 was activated, while 13 proteins were downregulated when CCCP was activated. TMPO, GPI, and RAB5C proteins were found in both autophagy and mitophagy, but they were more abundant in autophagy than in mitophagy. HSPA8 is another well-known significant protein that, while upregulated in autophagy, is downregulated in mitophagy. As a result, it is a novel protein that has never been linked to ATG3 in previous studies.

In conclusion, ATG3 plays an important role in cellular processes and is implicated in a variety of diseases, including cancer and neurodegenerative diseases. Although many studies have clarified interactions and structural basis, the specific mechanism necessitated further investigation. ATG3 is overexpressed in many cancer cell types, including solid tumors such as NSCLC. Because ATG3 is upregulated and results in increased autophagic flux, it may provide a survival advantage for solid tumors. As a result, ATG3 modulators may be a target for tumor progression. The identification of novel ATG3 interaction partners and the distinctions between autophagy and mitophagy add to the current body of knowledge. This may further contribute to detect ATG3's activity in various pathways.

6. CONCLUSION

The most important step in autophagy is autophagosome formation, which is carried out by approximately 40 ATG proteins known to date. Among these, ATG3 is required for both the ATG12 conjugation system and the ATG8/LC3 lipidation system which are both required for phagophore elongation. Therefore, the discovery of ATG3's binding partners will lead to a better understanding of phagophore formation and the cellular progression of many diseases.

In our study, we used GFP-TRAP pull-down assays and LC-MS/MS-based approaches to identify ATG3 partner proteins. We identified previously described binding partners of ATG3 including ATG12, ATG5, ATG7, ATG16L1, and LC3 proteins. In addition, we discovered a new partner GABARAPL2 protein in our experimental groups. The functional link between GABARAPL2 and ATG3 is currently not known and is in the scope of a future study. Furthermore, future research should look into the possibility of ATG3 interacting directly with RER1, RB1CC1, and HSPA8.

7. REFERENCES

1. Yang Z, Klionsky DJ. An Overview of the Molecular Mechanism of Autophagy. In 2009.
2. Bakula D, Müller AJ, Zuleger T, Takacs Z, Franz-Wachtel M, Thost AK, et al. WIPI3 and WIPI4 β-propellers are scaffolds for LKB1-AMPK-TSC signalling circuits in the control of autophagy. Nat Commun. 2017;8.
3. Dikic I, Elazar Z. Mechanism and medical implications of mammalian autophagy. Vol. 19, Nature Reviews Molecular Cell Biology. 2018. p. 349–64.
4. Kim HM, Kim ES, Koo JS. Expression of autophagy-related proteins in different types of thyroid cancer. Int J Mol Sci [Internet]. 2017 Mar 1 [cited 2022 Jan 5];18(3).
5. Deretic V, Saitoh T, Akira S. Autophagy in infection, inflammation and immunity. Vol. 13, Nature Reviews Immunology. 2013. p. 722–37.
6. Yang Z, Klionsky DJ. Mammalian autophagy: Core molecular machinery and signaling regulation. Current Opinion in Cell Biology. 2010.
7. Mizushima N, Levine B, Cuervo AM, Klionsky DJ. Autophagy fights disease through cellular self-digestion. Nature. 2008.
8. Ravikumar B, Sarkar S, Davies JE, Futter M, Garcia-Arencibia M, Green-Thompson ZW, et al. Regulation of mammalian autophagy in physiology and pathophysiology. Physiological Reviews. 2010.
9. Anding AL, Baehrecke EH. Autophagy in cell life and cell death. In: Current Topics in Developmental Biology. 2015.
10. Nixon RA. The role of autophagy in neurodegenerative disease. Nature Medicine. 2013.
11. Nordgren M, Wang B, Apanasets O, Fransen M. Peroxisome degradation in mammals: Mechanisms of action, recent advances, and perspectives. Front Physiol. 2013;
12. Maejima Y, Kyoi S, Zhai P, Liu T, Li H, Ivessa A, et al. Mst1 inhibits autophagy by promoting the interaction between beclin1 and Bcl-2. Nat Med. 2013;
13. Yang Z, Klionsky DJ. Eaten alive: A history of macroautophagy. Nature Cell Biology. 2010.
14. Orenstein SJ, Cuervo AM. Chaperone-mediated autophagy: Molecular mechanisms and physiological relevance. Seminars in Cell and Developmental Biology. 2010.
15. Fred Dice J. Peptide sequences that target cytosolic proteins for lysosomal proteolysis. Trends Biochem Sci. 1990;
16. Klionsky YC and DJ. The regulation of autophagy unanswered questions. 2011. p. 161–70.
17. Hayashi-Nishino M, Fujita N, Noda T, Yamaguchi A, Yoshimori T, Yamamoto A. A subdomain of the endoplasmic reticulum forms a cradle for autophagosome formation. Nat Cell Biol. 2009;11(12):1433–7.
18. Russell RC, Tian Y, Yuan H, Park HW, Chang YY, Kim J, et al. ULK1 induces autophagy by phosphorylating Beclin-1 and activating VPS34 lipid kinase. Nat Cell Biol. 2013;
19. Wirth M, Joachim J, Tooze SA. Autophagosome formation-The role of ULK1 and Beclin1-

PI3KC3 complexes in setting the stage. Seminars in Cancer Biology. 2013.

20. Alers S, Löffler AS, Wesselborg S, Stork B. The incredible ULKs. Cell Communication and Signaling. 2012.
21. Di Paolo G, De Camilli P. Phosphoinositides in cell regulation and membrane dynamics. Nature. 2006.
22. Tooze SA. Current views on the source of the autophagosome membrane. Essays Biochem. 2013;
23. Roberts R, Ktistakis NT. Omegasomes: PI3P platforms that manufacture autophagosomes. Essays Biochem. 2013;
24. He C, Klionsky DJ. Regulation mechanisms and signaling pathways of autophagy. Annu Rev Genet. 2009;43:67–93.
25. Mijaljica D, Prescott M, Devenish RJ. The intriguing life of Autophagosomes. Int J Mol Sci. 2012;13(3):3618–35.
26. Tanida I, Mizushima N, Kiyooka M, Ohsumi M, Ueno T, Ohsumi Y, et al. Apg7p/Cvt2p: A novel protein-activating enzyme essential for autophagy. Mol Biol Cell. 1999;
27. Shintani T, Mizushima N, Ogawa Y, Matsuura A, Noda T, Ohsumi Y. Apg10p, a novel protein-conjugating enzyme essential for autophagy in yeast. EMBO J. 1999;
28. Mizushima N, Noda T, Yoshimori T, Tanaka Y, Ishii T, George MD, et al. A protein conjugation system essential for autophagy. Nature. 1998;
29. Carlsson SR, Simonsen A. Membrane dynamics in autophagosome biogenesis. Journal of Cell Science. 2015.
30. Mizushima N, Ohsumi Y, Yoshimori T. Autophagosome formation in mammalian cells. Cell Structure and Function. 2002.
31. Poole AC, Thomas RE, Andrews LA, McBride HM, Whitworth AJ, Pallanck LJ. The PINK1/Parkin pathway regulates mitochondrial morphology. Proc Natl Acad Sci U S A. 2008;
32. Klionsky DJ, Abdelmohsen K, Abe A, Abedin MJ, Abeliovich H, Arozena AA, et al. Guidelines for the use and interpretation of assays for monitoring autophagy (3rd edition). Autophagy. 2016.
33. Stolz A, Ernst A, Dikic I. Cargo recognition and trafficking in selective autophagy. Nature Cell Biology. 2014.
34. Rogov V, Dötsch V, Johansen T, Kirkin V. Interactions between Autophagy Receptors and Ubiquitin-like Proteins Form the Molecular Basis for Selective Autophagy. Molecular Cell. 2014.
35. Shen HM, Mizushima N. At the end of the autophagic road: An emerging understanding of lysosomal functions in autophagy. Trends in Biochemical Sciences. 2014.
36. Itakura E, Kishi-Itakura C, Mizushima N. The hairpin-type tail-anchored SNARE syntaxin 17 targets to autophagosomes for fusion with endosomes/lysosomes. Cell. 2012;151(6):1256–69.
37. Yu L, Chen Y, Tooze SA. Autophagy pathway: Cellular and molecular mechanisms. Autophagy. 2018;14(2):207–15.
38. Ponpuak M, Mandell MA, Kimura T, Chauhan S, Cleyrat C, Deretic V. Secretory autophagy.

Current Opinion in Cell Biology. 2015.

39. Berg TO, Fengsrud M, Strømhaug PE, Berg T, Seglen PO. Isolation and characterization of rat liver amphisomes: Evidence for fusion of autophagosomes with both early and late endosomes. J Biol Chem. 1998;
40. Sanchez-Wandelmer J, Reggiori F. Amphisomes: Out of the autophagosome shadow? EMBO J. 2013;
41. Rubinsztein DC, Gestwicki JE, Murphy LO, Klionsky DJ. Potential therapeutic applications of autophagy. Nat Rev Drug Discov. 2007;6(4):304–12.
42. Williams A, Jahreiss L, Sarkar S, Saiki S, Menzies FM, Ravikumar B, et al. Aggregate-Prone Proteins Are Cleared from the Cytosol by Autophagy: Therapeutic Implications. Vol. 76, Current Topics in Developmental Biology. Academic Press; 2006. p. 89–101.
43. Crighton D, Wilkinson S, O'Prey J, Syed N, Smith P, Harrison PR, et al. DRAM, a p53-Induced Modulator of Autophagy, Is Critical for Apoptosis. Cell. 2006;126(1):121–34.
44. Feng Z, Zhang H, Levine AJ, Jin S. The coordinate regulation of the p53 and mTOR pathways in cells. Proc Natl Acad Sci U S A. 2005;102(23):8204–9.
45. Levine B, Kroemer G. Autophagy in the Pathogenesis of Disease. Vol. 132, Cell. 2008. p. 27–42.
46. Dunker AK, Lawson JD, Brown CJ, Williams RM, Romero P, Oh JS, et al. Intrinsically disordered protein. J Mol Graph Model. 2001;
47. Wright PE, Dyson HJ. Intrinsically unstructured proteins: Re-assessing the protein structure-function paradigm. J Mol Biol. 1999;
48. Kragelj J, Ozenne V, Blackledge M, Jensen MR. Conformational propensities of intrinsically disordered proteins from NMR chemical shifts. ChemPhysChem. 2013.
49. Tompa P. The interplay between structure and function in intrinsically unstructured proteins. FEBS Letters. 2005.
50. Cumberworth A, Lamour G, Babu MM, Gsponer J. Promiscuity as a functional trait: Intrinsically disordered regions as central players of interactomes. Biochemical Journal. 2013.
51. Mao AH, Lyle N, Pappu R V. Describing sequence-ensemble relationships for intrinsically disordered proteins. Biochemical Journal. 2013.
52. Babu MM, van der Lee R, de Groot NS, Gsponer J. Intrinsically disordered proteins: Regulation and disease. Current Opinion in Structural Biology. 2011.
53. Uversky VN, Oldfield CJ, Dunker AK. Intrinsically disordered proteins in human diseases: Introducing the D 2 concept. Annual Review of Biophysics. 2008.
54. Mei Y, Su M, Soni G, Salem S, Colbert CL, Sinha SC. Intrinsically disordered regions in autophagy proteins. Proteins Struct Funct Bioinforma. 2014;
55. Tantos A, Han KH, Tompa P. Intrinsic disorder in cell signaling and gene transcription. Molecular and Cellular Endocrinology. 2012.
56. Oral O, Oz-Arslan D, Itah Z, Naghavi A, Deveci R, Karacali S, et al. Cleavage of Atg3 protein by caspase-8 regulates autophagy during receptor-activated cell death. Apoptosis.

2012;17(8):810–20.

57. Tanida I, Nishitani T, Nemoto T, Ueno T, Kominami E. Mammalian Apg12p, but not the Apg12p Á Apg5p conjugate, facilitates LC3 processing q. Biochem Biophys Res Commun [Internet]. 2002 [cited 2021 Sep 9];296:1164–70.
58. Yamada Y, Suzuki NN, Hanada T, Ichimura Y, Kumeta H, Fujioka Y, et al. The Crystal Structure of Atg3, an Autophagy-related Ubiquitin Carrier Protein (E2) Enzyme that Mediates Atg8 Lipidation. J Biol Chem. 2007;282(11):8036–43.
59. Popelka H, Uversky VN, Klionsky DJ. Identification of Atg3 as an intrinsically disordered polypeptide yields insights into the molecular dynamics of autophagy-related proteins in yeast. autophagy 1093 autophagy. 2014;10(6):1093–104.
60. Varshavsky A. The ubiquitin system [Internet]. Vol. 22, Trends in Biochemical Sciences. Elsevier; 1997 p. 383–7.
61. Tanida I, Tanida-Miyake E, Komatsu M, Ueno T, Kominami E. Human Apg3p/Aut1p Homologue Is an Authentic E2 Enzyme for Multiple Substrates, GATE-16, GABARAP, and MAP-LC3, and Facilitates the Conjugation of hApg12p to hApg5p*. 2002
62. Sugawara K, Suzuki NN, Fujioka Y, Mizushima N, Ohsumi Y, Inagaki F. The crystal structure of microtubule-associated protein light chain 3, a mammalian homologue of Saccharomyces cerevisiae Atg8.
63. Kirisako T, Ichimura Y, Okada H, Kabeya Y, Mizushima N, Yoshimori T, et al. The Reversible Modification Regulates the Membrane-Binding State of Apg8/Aut7 Essential for Autophagy and the Cytoplasm to Vacuole Targeting Pathway. Vol. 151, The Journal of Cell Biology. 2000.
64. Sugawara K, Suzuki NN, Fujioka Y, Mizushima N, Ohsumi Y, Inagaki F. Structural basis for the specificity and catalysis of human Atg4B responsible for mammalian autophagy. J Biol Chem. 2005;280(48):40058–65.
65. Ohsumi Y. Genetic approaches to autophagy in yeast. Nat Rev Mol Cell Biol [Internet]. 2001;2(March):211–6.
66. Moloughney JG, Monken CE, Tao H, Zhang H, Thomas JD, Lattime EC, et al. Vaccinia virus leads to ATG12-ATG3 conjugation and deficiency in autophagosome formation. 2011;7(12):1434–47.
67. Chang TK, Shravage B V., Hayes SD, Powers CM, Simin RT, Wade Harper J, et al. Uba1 functions in Atg7- and Atg3-independent autophagy. Vol. 15, Nature Cell Biology. 2013. p. 1067–78.
68. Radoshevich L, Murrow L, Chen N, Fernandez E, Roy S, Fung C, et al. ATG12 conjugation to ATG3 regulates mitochondrial homeostasis and cell death. Cell. 2010;142(4):590–600.
69. Altman BJ, Jacobs SR, Mason EF, Michalek RD, MacIntyre AN, Coloff JL, et al. Autophagy is essential to suppress cell stress and to allow BCR-Abl-mediated leukemogenesis. Vol. 30, Oncogene. 2011. p. 1855–67.
70. Choi J, Park S, Biering SB, Selleck E, Liu CY, Fujita N, et al. The parasitophorous vacuole membrane of Toxoplasma gondii is targeted for disruption by ubiquitin-like conjugation

systems of autophagy. 2015;40(6):924–35.

71. Hervás JH, Landajuela A, Antón Z, Shnyrova A V, Goñi FM, Alonso A. Human ATG3 binding to lipid bilayers: Role of lipid geometry, and electric charge. Sci Rep. 2017;7(1):1–15.
72. Zhuang L, Ma Y, Wang Q, Zhang J, Zhu C, Zhang L, et al. Atg3 overexpression enhances bortezomib-induced cell death in SKM-1 cell. PLoS One. 2016;11(7):1–16.
73. Management C, Huang W, Zeng C, Hu S, Wang L, Liu J. ATG3, a Target of miR-431-5p, Promotes Proliferation and Invasion of Colon Cancer via Promoting Autophagy. 2019;
74. Wang H, Zhang Y, Wu Q, Wang Y, Wang W. miR-16 mimics inhibit TGF- β 1-induced epithelial-to-mesenchymal transition via activation of autophagy in non-small cell lung carcinoma cells. 2018;247–54.
75. Saitoh T, Fujita N, Jang MH, Uematsu S, Yang B, Satoh T, et al. Loss of the autophagy protein Atg16L1 enhances endotoxin-induced IL-1 b production. 2008;456(November).
76. Yu-shin Sou, Satoshi Waguri,Jun-ichi Iwata,Takashi Ueno, Tsutomu Fujimura, Taichi Hara, Naoki Sawada AY, Noboru Mizushima, Yasuo Uchiyama, Eiki Kominami KT, Komatsu and M. The Atg8 Conjugation System Is Indispensable for Proper Development of Autophagic Isolation Membranes in Mice. Mol Biol Cell. 2008;Vol. 19, 4(November):1–14.
77. Liu P, Liu K, Gu H, Wang W, Gong J, Zhu Y, et al. High autophagic flux guards ESC identity through coordinating autophagy machinery gene program by FOXO1. Cell Death Differ. 2017 Oct 16;24(10):1672–80.
78. Ma K, Fu W, Tang M, Zhang C, Hou T, Li R, et al. PTK2-mediated degradation of ATG3 impedes cancer cells susceptible to DNA damage treatment. Autophagy. 2017;13(3):579–91.
79. Wang T, Yu N, Qian M, Feng J, Cao S, Yin J, et al. ERK-mediated autophagy promotes inactivated Sendai virus (HVJ-E)-induced apoptosis in HeLa cells in an Atg3-dependent manner. Vol. 18, Cancer Cell International. 2018.
80. Liu T, Fang H, Liu J, Reid S, Hou J, Zhou T, et al. Cytosolic glyceraldehyde-3-phosphate dehydrogenases play crucial roles in controlling cold-induced sweetening and apical dominance of potato (Solanum tuberosum L.) tubers. Plant Cell Environ. 2017;40(12):3043–54.
81. Liu Y, Schiff M, Czymmek K, Tallóczy Z, Levine B, Dinesh-Kumar SP. Autophagy regulates programmed cell death during the plant innate immune response. Cell. 2005;121(4):567–77.
82. Yamashita SI, Kanki T. How autophagy eats large mitochondria: Autophagosome formation coupled with mitochondrial fragmentation. Autophagy. 2017;13(5):980–1.
83. LEMASTERS JJ. Perspective Selective Mitochondrial Autophagy, or Mitophagy, as a Targeted Defense Against Oxidative Stress, Mitochondrial Dysfunction, and Aging. 2005;8(1):3–5.
84. Hom J, Sheu SS. Morphological dynamics of mitochondria - A special emphasis on cardiac muscle cells. J Mol Cell Cardiol. 2009;46(6):811–20.
85. Zhao RUZ, Jiang S, Zhang LIN, Yu ZHIBIN. Mitochondrial electron transport chain, ROS generation and uncoupling (Review). 2019;3–15.
86. Porter GA, Hom JR, Hoffman DL, Quintanilla RA, Mesy KL De, Sheu S. Progress in Pediatric Cardiology Bioenergetics, mitochondria, and cardiac myocyte differentiation. Prog Pediatr

Cardiol. 2011;31(2):75–81.

87. Wang S, Deng Z, Ma Y, Jin J, Qi F, Li S, et al. The Role of Autophagy and Mitophagy in Bone Metabolic Disorders. 2020;16.

88. Westermann B. Mitochondrial fusion and fission in cell life and death. Nat Publ Gr. 2010;11(12):872–84.

89. Taylor P, Atg ATG, Radoshevich L, Debnath J. Autophagy ATG12-ATG3 and mitochondria. 2011;(August 2015):5–8.

90. Besteiro S, Brooks CF, Striepen B, Dubremetz JF. Autophagy protein Atg3 is essential for maintaining mitochondrial integrity and for normal intracellular development of toxoplasma gondii tachyzoites. PLoS Pathog. 2011;7(12).

91. Cai J, Pires KM, Ferhat M, Chaurasia B, Buffolo MA, Smalling R, et al. Autophagy Ablation in Adipocytes Induces Insulin Resistance and Reveals Roles for Lipid Peroxide and Nrf2 Signaling in Adipose-Liver Crosstalk. Cell Rep. 2018;25(7):1708-1717.e5.

92. Liu K, Zhao Q, Liu P, Cao J, Gong J, Wang C, et al. ATG3-dependent autophagy mediates mitochondrial homeostasis in pluripotency acquirement and maintenance. 2016;8627(August).

93. Baker F, Polat IH, Abou-El-Ardat K, Alshamleh I, Thoelken M, Hymon D, et al. Metabolic Rewiring Is Essential for AML Cell Survival to Overcome Autophagy Inhibition by Loss of ATG3. Cancers (Basel). 2021;13:6142.

94. Ruas JS, Siqueira-santos ES, Amigo I, Rodrigues-silva E. Underestimation of the Maximal Capacity of the Mitochondrial Electron Transport System in Oligomycin-Treated Cells. 2016;1–20.

95. Itakura E, Kishi-Itakura C, Koyama-Honda I, Mizushima N. Structures containing Atg9A and the ULK1 complex independently target depolarized mitochondria at initial stages of Parkin-mediated mitophagy. J Cell Sci. 2012;125(6):1488–99.

96. Matthiesen R, Mutenda KE. Introduction to proteomics. Methods Mol Biol. 2007;367:1–35.

97. Jung ME, Kim WJ, Avliyakulov NK, Oztug M, Haykinson MJ. Synthesis and validation of cyanine-based dyes for DIGE. Methods Mol Biol. 2012;854:67–85.

98. Popelka H, Uversky VN, Klionsky DJ. Identification of Atg3 as an intrinsically disordered polypeptide yields insights into the molecular dynamics of autophagy-related proteins in yeast. 2014;(June):1093–104.

99. Narendra RJY and DP. Mechanisms of mitophagy. Nature Publishing Group. 2011.

100. Tanida I, Ueno T, Kominami E. LC3 and autophagy. Methods Mol Biol. 2008;445(2):77–88.

101. Xu S, Li L, Li M, Zhang M, Ju M, Chen X, et al. Impact on Autophagy and Ultraviolet B Induced Responses of Treatment with the MTOR Inhibitors Rapamycin, Everolimus, Torin 1, and pp242 in Human Keratinocytes. Das A, editor. Oxid Med Cell Longev. 2017;2017:5930639.

102. Gómez-Sánchez R, Gegg ME, Bravo-San Pedro JM, Niso-Santano M, Alvarez-Erviti L, Pizarro-Estrella E, et al. Mitochondrial impairment increases FL-PINK1 levels by calcium-dependent gene expression. Neurobiol Dis [Internet]. 2014;62:426–40.

103. Pospiech N, Cibis H, Dietrich L, Müller F, Bange T, Hennig S. Identification of novel PANDAR

protein interaction partners involved in splicing regulation. Sci Rep. 2018;8(1):2–10.

104. Hunter MR, Hesketh GG, Benedyk TH, Gingras AC, Graham SC. Proteomic and Biochemical Comparison of the Cellular Interaction Partners of Human VPS33A and VPS33B. J Mol Biol [Internet]. 2018 Jul 6 [cited 2022 Jan 6];430(14):2153–63.
105. Gavin AC, Maeda K, Kühner S. Recent advances in charting protein–protein interaction: mass spectrometry-based approaches. Curr Opin Biotechnol. 2011 Feb 1;22(1):42–9.
106. Richards AL, Eckhardt M, Krogan NJ. Mass spectrometry-based protein-protein interaction networks for the study of human diseases. Mol Syst Biol. 2021;17:8792.
107. Taha MS, Haghighi F, Stefanski A, Nakhaei-Rad S, Kazemein Jasemi NS, Al Kabbani MA, et al. Novel FMRP interaction networks linked to cellular stress. Vol. 288, FEBS Journal. 2021. 837–860 p.
108. Wang F, Wu H, Zhang S, Lu J, Lu Y, Zhan P, et al. LAPTM4B facilitates tumor growth and induces autophagy in hepatocellular carcinoma. 2019; Available from: http://doi.org/10.2147/CMAR.S201092
109. Lubas M, Harder LM, Kumsta C, Tiessen I, Hansen M, Andersen JS, et al. eIF5A is required for autophagy by mediating ATG3 translation.
110. Nguyen TN, Padman BS, Usher J, Oorschot V, Ramm G, Lazarou M. Atg8 family LC3/GABARAP proteins are crucial for autophagosome-lysosome fusion but not autophagosome formation during PINK1/Parkin mitophagy and starvation. J Cell Biol. 2016;215(6):857–74.
111. Ghavidel A, Baxi K, Ignatchenko V, Prusinkiewicz M, Arnason TG, Kislinger T, et al. A Genome Scale Screen for Mutants with Delayed Exit from Mitosis: Ire1-Independent Induction of Autophagy Integrates ER Homeostasis into Mitotic Lifespan. 2015;
112. Yamano K, Youle RJ. Two different axes CALCOCO2-RB1CC1 and OPTN-ATG9A initiate PRKN-mediated mitophagy.

8. CURRICULUM VITAE